Forest Ecosystems 9 (2022) 100080

Contents lists available at ScienceDirect

Forest Ecosystems

journal homepage: www.keaipublishing.com/cn/journals/forest-ecosystems

Automated registration of wide-baseline point clouds in forests using discrete overlap search

Onni Pohjavirta [a,1], Xinlian Liang [b,a,1,*], Yunsheng Wang [a], Antero Kukko [a], Jiri Pyörälä [a,c], Eric Hyyppä [a], Xiaowei Yu [a], Harri Kaartinen [a,d], Juha Hyyppä [a]

[a] Department of Remote Sensing and Photogrammetry, Finnish Geospatial Research Institute, Vuorimiehentie 5, Espoo, 02150, Finland
[b] The State Key Laboratory of Information Engineering in Surveying, Mapping and Remote Sensing, Wuhan University, Wuhan, 430070, China
[c] Department of Forest Sciences, University of Helsinki, Helsinki, FI-00014, Finland
[d] Department of Geography and Geology, University of Turku, Turku, FI-20500, Finland

ARTICLE INFO

Keywords:
Close-range sensing
Forest
Registration
Point cloud
Wide-baseline
Terrestrial laser scanning
Unmanned aerial vehicle
Drone
In situ
Discrete overlap search

ABSTRACT

Forest is one of the most challenging environments to be recorded in a three-dimensional (3D) digitized geometrical representation, because of the size and the complexity of the environment and the data-acquisition constraints brought by on-site conditions. Previous studies have indicated that the data-acquisition pattern can have more influence on the registration results than other factors. In practice, the ideal short-baseline observations, i.e., the dense collection mode, is rarely feasible, considering the low accessibility in forest environments and the commonly limited labor and time resources. The wide-baseline observations that cover a forest site using a few folds less observations than short-baseline observations, are therefore more preferable and commonly applied. Nevertheless, the wide-baseline approach is more challenging for data registration since it typically lacks the required sufficient overlaps between datasets. Until now, a robust automated registration solution that is independent of special hardware requirements has still been missing. That is, the registration accuracy is still far from the required level, and the information extractable from the merged point cloud using automated registration could not match that from the merged point cloud using manual registration. This paper proposes a discrete overlap search (DOS) method to find correspondences in the point clouds to solve the low-overlap problem in the wide-baseline point clouds. The proposed automatic method uses potential correspondences from both original data and selected feature points to reconstruct rough observation geometries without external knowledge and to retrieve precise registration parameters at data-level. An extensive experiment was carried out with 24 forest datasets of different conditions categorized in three difficulty levels. The performance of the proposed method was evaluated using various accuracy criteria, as well as based on data acquired from different hardware, platforms, viewing perspectives, and at different points of time. The proposed method achieved a 3D registration accuracy at a 0.50-cm level in all difficulty categories using static terrestrial acquisitions. In the terrestrial-aerial registration, data sets were collected from different sensors and at different points of time with scene changes, and a registration accuracy at the raw data geometric accuracy level was achieved. These results represent the highest automated registration accuracy and the strictest evaluation so far. The proposed method is applicable in multiple scenarios, such as 1) the global positioning of individual under-canopy observations, which is one of the main challenges in applying terrestrial observations lacking a global context, 2) the fusion of point clouds acquired from terrestrial and aerial perspectives, which is required in order to achieve a complete forest observation, 3) mobile mapping using a new stop-and-go approach, which solves the problems of lacking mobility and slow data collection in static terrestrial measurements as well as the data-quality issue in the continuous mobile approach. Furthermore, this work proposes a new error estimate that units all parameter-level errors into a single quantity and compensates for the downsides of the widely used parameter- and object-level error estimates; it also proposes a new deterministic point sets registration method as an alternative to the popular sampling methods.

* Corresponding author. The State Key Laboratory of Information Engineering in Surveying, Mapping and Remote Sensing, Wuhan University, Wuhan, 430070, China.
E-mail address: xinlian.liang@whu.edu.cn (X. Liang).
[1] Xinlian Liang and Onni Pohjavirta are the joint first authors.

https://doi.org/10.1016/j.fecs.2022.100080
Received 17 August 2022; Received in revised form 1 December 2022; Accepted 1 December 2022

1. Introduction

Point cloud registration, also known as point set matching, aims to find spatial transformation or mapping parameters to align point sets into a common reference frame. Finding sufficient correspondences between observations is vital for a successful registration, but it is not always straightforward, depending on the data, the data-acquisition approaches and the applied scenarios.

From the data point of view, the point clouds involved in the registration can be targeted at the same object or different objects with similarities, and can be collected from different viewpoints, with different sensors, and/or at multiple points of time. Among these, the registration between point clouds of the same objects from different points of view is the most widely studied subject in order to build a comprehensive digitization of the study objects, where sensor, temporal, and objects change are not considered.

From the transformation point of view, the types of spatial transformation can be rigid or non-rigid (Crum et al., 2004; Tam et al., 2013). A rigid transformation preserves the distances between point pairs in a point cloud whereas a non-rigid transformation projects one point set to another with varying discrepancies or localized stretching. During the last a few decades, because of the rapid progress in the availability and quality of ranging sensors, the rigid registration has received close attention in order to promote the understanding and applications of rich point cloud data.

From the data-acquisition point of view, registration works with both short- and wide-baseline observations, i.e., dense and sparse data-acquisition settings. The short-baseline observations have small distances between viewpoints, small differences in viewing geometries, and large overlaps between observations. These consequently increase the probability of finding correspondences to support a successful matching. Short baselines are typically applied in online applications (Durrant--Whyte and Bailey, 2006; Magnusson et al., 2007), aiming primarily on determining the platform location and on navigating the platform in automation, navigation, robotics, and mobile geomatics. When applied offline, the focus is primarily on optimizing the trajectory to improve the localization and even the mapping accuracy (Borrmann et al., 2008).

The wide-baseline observations keep the number of measurements low due to practical concerns (Pomerleau et al., 2015). With wide-baseline or sparse observations, the same area can be covered with considerably so that there is no repetition fewer observations than with dense observations. Thus, it significantly reduces the costs and workload, and becomes the preferable solution whenever it is applicable, e.g., in applications with a limited budget or in environments with restricted accessibility. However, wide-baseline observations are characterized by significant changes in views between observations, and they consequently lack similarities and large overlaps between views that are typically required in registration. Thus, the wide-baseline observations are easy to implement in the field but they are more challenging for the post-processing.

Considering the applied scenario, complicated scenes lead to ubiquitous occlusion effects. Different viewpoints, occlusion effects, and low overlaps between point pairs lead to limited one-to-one correspondences (Tam et al., 2013). A clear visibility increases the possibility of a successful registration, and vice versa. The complicated structures and occlusion effects may significantly reduce the visibility in each point cloud and the potential to find correct correspondences. As shown in a recent study, the registration completely failed when the majority of the structural objects in a point set were occluded (Tremblay and Béland, 2018). Perturbation from moving objects, i.e., trees and other vegetation swayed by the wind, that prevails in practical scenarios, particularly in forest and other environment conditions (Vaaja et al., 2016; Pyörälä et al., 2019), further leads to false correspondences and introduces structured and unstructured outliers. More discussion on the challenges of the point-cloud registration in forests is in Section 2.

Overall, the complexity of a registration problem is jointly determined by all four elements, i.e., the data, transformation type, data-acquisition approach, and applied scenario. The level of influence by each of these varies case by case. In a study using the dense data acquisition (Tremblay and Béland, 2018), the best results among five test sites were from the most complex site where the occlusion is the most significant but the distances between observation positions were the shortest. This result suggested that there are trade-offs among the impacting elements. For example, a trade-off exists between the sparseness of the data-acquisition network and the success rate of the registration, i.e., the baseline between observation positions should be kept short to avoid excessive occlusion. It also highlighted that the data-acquisition pattern can have an even greater influence on the registration results than the algorithm and the on-site conditions. Namely, achieving an accurate registration in difficult forest conditions may be relatively easy using the dense sensing pattern, while it may be challenging in easy forest conditions using the sparse pattern.

Given these technical and practical difficulties, an automated data-level registration solution needs to answer three fundamental questions to overcome the challenges in point-cloud registration. Namely, 1) what features or points to employ in the matching, especially in environments where the data and/or the objects are generally incomplete and fragmented, 2) how to establish correspondences between data sets, especially those with limited overlap and uniqueness, and 3) how to achieve an accurate and robust registration, especially in the presence of large amounts of structured outliers and in varying conditions.

Thus far, these questions have not been adequately answered. Especially, the applicability of the so far proposed methods remains unknown, as a proper evaluation of the registration algorithms is constantly missing (Liang et al., 2022). In short, the automated registration in forests, especially using wide-baseline observations, still lacks accurate and applicable solutions and requires further discussion from the methodology and applicability perspectives.

This work proposes an automatic point-cloud registration method to match wide-baseline point cloud observations in boreal forest environments. Specifically, this work proposes 1) a new two-dimensional (2D) point set registration method, which works in noisy data sets and is a deterministic method that eliminates the uncertainty in repeated sampling methods, 2) a new and general framework to find correspondences to solve the problem related to the low overlap, i.e., discrete overlap search (DOS) method, 3) a new type of evaluation criterion that compensates for the downsides of the parameter- and object-level error estimates by uniting all parameter-level errors into a single quantity, i.e., an error upper bound based on reference registration parameters that quantitatively indicates the largest pointwise registration uncertainty at any spatial position when applying a particular set of registration parameters, and 4) a new type of mobile mapping approach, the stop-and-go mode, where the platform moves similarly to a mobile mapping system but the data are collected similarly to a static system, i.e., at selected positions as opposed to the continuous mobile-mapping approach where data acquisition takes place all the time along the trajectory. Compared to the static approach such as Terrestrial Laser Scanning (TLS) where the scanner is moved by a human operator, the stop-and-go allows automated data collection and higher efficiency. Until now, the application of the stop-and-go mode has not been feasible in practice because the data acquisition speed is too low as the accurate and automated registration has required short distances between observations.

This work presents the so far most comprehensive and strict evaluation for an automated registration algorithm in diverse forest conditions. The proposed method was tested with 24 datasets in boreal forests. The forests have significant variability in age, development stages, species composition, ground surface roughness/inclination, etc., thus representing different levels of difficulty in registration. The performance of the proposed algorithm was evaluated based on accurate reference data, three quantitative criteria, and the variation of input parameter values. The applicability of the proposed algorithm was also demonstrated by applying the algorithm to point clouds from both single and multiple

sensors, platforms, points of time with scene changes, and different viewpoints, i.e., the terrestrial and aerial viewpoints, which showed that the proposed method is applicable to a wide-range of point-cloud data as long as the sensors provide sufficiently accurate data.

In terms of the achieved registration accuracy, the proposed algorithm improves the state-of-the-art results by an order of magnitude, i.e., the accuracy is roughly 10 times better than that in the previous studies. The mean target-wise *XY*, *Z* and *XYZ* errors in the terrestrial viewpoint were 0.32, 0.34 and 0.48 cm at the plot level. Considering that the scanner measurement accuracy is at the millimeter level, the achieved registration accuracy is close to the accuracy of the raw point cloud and close to the accuracy achieved using reference targets which is arguably the highest accuracy that can be achieved. Meanwhile, forest stand complexity and perturbation in the parameter values appear to have a limited impact on the algorithm performance, which indicates that the proposed method is robust with respect to the parameter values in most of the investigated forest stand conditions.

The proposed method is applicable in multiple scenarios, such as 1) the global positioning of individual under-canopy observations, which is one of the main challenges in applying terrestrial observations that lack a global context, 2) the fusion of point clouds acquired from terrestrial and aerial perspectives, which is required in order to achieve a complete forest observation and is challenging because of significant differences in the observation geometries 3) mobile mapping using a new stop-and-go approach, which solves the problems of lacking mobility and low data-acquisition efficiency in static terrestrial measurements as well as the low data-quality problem in the continuous mobile approach.

In addition, the reported accuracy from Terrestrial Laser Scanning (TLS) observations also serves as an upper bound for the accuracy that can be achieved from all point cloud sources, as the static TLS represents the best accuracy of all point clouds from different sources, e.g., mobile platforms and image-based point clouds (Liang et al., 2022).

The paper is organized as follows. Section 2 outlines the background, e.g., the sparse and dense data-acquisition patterns, the challenges that forest point cloud registration faces and the previous studies. Section 3 briefly presents the study material. Sections 4 and 5 present the registration algorithm and the experiment results. The discussion concerning the method, results, evaluation, applicability in forest environments and future work is presented in Section 6. Findings are summarized in Section 7.

2. State-of-the-art and current challenges

The registration of point clouds in forests has the same aim and follows the similar processing principles as the general point-set matching solutions. However, the forest conditions, as well as the wide baselines, pose significant challenges for the registration, especially the conditions of the omnipresent occlusion effects and the self-similarities. This section outlines the current status of the forest registration research, including the sparse and dense data-acquisition patterns, challenges, and previous studies.

2.1. Sparse and dense data acquisition

The main difference between the sparse and dense data-acquisition patterns lies in the way the observation network is established. The sparse pattern aims to capture the target scene or object efficiently with only a few limited observations, resulting in wide baselines between the scans. The dense data-acquisition primarily aims at recording the environment comprehensively with an intensive short-baseline observation network.

For example, to cover a typical sample plot in boreal forest conditions, the sparse setting typically uses a few observations with a baseline of 10 m or more, whereas the dense data-acquisition approach uses dozens of observation positions with a shorter baseline, e.g., 5 m or less.

Table 1 compares a few theoretical scanning setups following uniform grids with different baselines d in 60 m × 60 m and 10 m × 100 m plots, respectively. The scan density D is defined as $:= \lim_{A\to\infty} \frac{N_{A,d}}{A} = \frac{1}{d^2}$, where A is the area of a square plot and $N_{A,d}$ is the number of scans within the plot following a uniform grid with baseline d.

In the 60 m × 60 m plot, the dense sensing pattern with 5-m baseline requires approximately 3–10 times more scans than the sparse sensing with 10–20 m baseline. Based on the scan density, dense sensing can require 4 to 16 times more scans in larger plot areas than the sparse sensing.

It is worth to mention that the theoretical scanning setups in Table 1 are purely based on evaluating the scan density D with different inputs d, and the values are not bounded to any specific scanner.

In general, a baseline above 10 m follows a sparse data-acquisition pattern and below 5 m follows a dense pattern, which in terms of the density correspond to less than 100 and more than 400 scans per ha, respectively. Nevertheless, the division between the sparse and dense patterns is less strict. For example, 300 scans per ha, i.e., 5.8-m baseline, is still considered dense and 150 scans per ha, i.e., 8.2-m baseline, sparse.

As the dense pattern uses a few times more observation positions in the data-acquisition network than the sparse setting, the cost of the dense setting is also in principle many times more than that of the sparse acquisition. Thus, practical concerns, i.e., the limited accessibility in forests and the lower costs in labor and time, lead to a preference of using the sparse data-acquisition setting over the dense sensing in forests. The choice between the sparse and dense networks is however site- and application-dependent. In the close proximity of highly occluding objects, such as steep hills, rocks and impenetrable vegetation, shorter baselines are probably the only choice in order to ensure sufficient overlap between neighboring scans.

2.2. Challenges

The challenges of the automated registration of forest scans stem from multiple perspectives, e.g., the complicated in situ conditions, the limited overlaps between observations, and the lack of prior knowledge on the observation geometry to name a few.

The forest environment is a scenario where the data is heavily disturbed by noise and has a limited number of features suitable for being used as matching targets. Points reflected from tree crowns and bushes comprise a large portion of the raw point cloud data but do not contain structured information required in an accurate registration. Structured objects, e.g., stems and ground, often lack representativeness as they present self-similarities in their immediate neighborhood, and thus may introduce false correspondences. For example, the shape and size of a tree-stem section may present little variance in the vertical direction, e.g., in a 1-m section (Liu et al., 2017).

Occlusion effects prevail in forests (Wang et al., 2019b), which reduces the overlap between point cloud data sets. At the plot level, a point cloud recorded at a single position barely records objects beyond 5 m from the viewing position in dense forest conditions (e.g., ~2000 stems·ha^{-1}) due to obstruction brought by vegetation close to the scanner (Liang et al., 2018a). For individual trees, the visibility sharply decreases along the tree growth direction due to the crown occlusion (Pyörälä et al.,

Table 1
A comparison of scan patterns over a theoretical plot area following different baselines. The scan locations are assumed to follow a uniform grid. The scan density represents the limit value of the number of scans per unit area.

Baseline (m)	Number of scans		Scan density (per ha)
	60 m × 60 m	100 m × 100 m	
5	169	441	400.0
10	49	121	100.0
15	25	49	44.4
20	16	36	25.0

2019; Wang et al., 2019a) and varies significantly in the horizontal direction (Liang et al., 2012; Saarinen et al., 2017). Consequently, forests commonly appear incomplete and fragmented in the recorded point clouds, particularly in those captured from a single viewpoint. As a result, identifying correspondences is challenging due to the lack of corresponding features among data sets.

The in situ environmental conditions further reduce the amount of useful information for registration purposes. Wind may move the tree stems and crowns (Vaaja et al., 2016; Pyörälä et al., 2019) so that identical features may be recorded at different spatial locations in point clouds from different viewpoints or at different points of time. These further reduce the number of correspondences between point clouds and turn useful targets into structured outliers.

The wide-baseline observations, which have significant variance in viewing geometries, can lead to small overlaps between data sets. Thus, few common points may exist between successive observations (Pomerleau et al., 2015). For two scans with 15-m baseline and 20-m coverage radii, the common planar area in the *XY* plane is 53% of the total area covered by each full field-of-view scan, without considering the occlusion effects and diversity in view geometries. Assuming the objects distribute evenly in the forest, only half of the objects and/or features in one point cloud have potential correspondences in the other. Thus, theoretically, at least half of the features in wide-baseline observations are outliers in the registration context, i.e., signal-to-noise ratio at 1:1 at best.

At the object level, taking the tree stems as an example, only the side facing the scanner is visible in data from a fixed viewing position. Therefore, a tree stem has a maximum coverage of 50%. Given the 50% theoretical maximum coverage of object surface in each scan, the common area in the datasets with different viewing geometries can be very limited even within the overlapping area between two point clouds. The common area is practically zero for objects between two scanning locations, because those objects are observed from the opposite directions. In short, the common objects and common coverage areas between two wide-baseline point clouds make up only a small portion of the raw data, i.e., less or much less than 50%.

The use of knowledge such as sensor positions, orientations, and distances from external sources can reduce the complexity in the registration problem by providing a rough viewing geometry. For example, exterior orientation devices can obtain approximate exterior orientations (Pfeifer and Briese, 2007), and GNSS can also collect relative positions, as shown in the research (Henning and Radtke, 2006, 2008; Ni et al., 2011; Hilker et al., 2012; Zhang et al., 2016).

However, the applicability of the exterior orientation devices largely depends on the hardware quality and availability. The task of collecting sensor positions using GNSS under forest canopy is not trivial either. The absolute positioning accuracy is currently at a 0.50-m level in boreal forest conditions (Kaartinen et al., 2015), depending heavily on the canopy density and satellite visibility. Since the availability of external knowledge is not guaranteed, the dependency on external knowledge limits the applicability of the registration algorithm.

2.3. Previous studies

This section reviews the studies on the sparse data-acquisition pattern that were implemented at data-, feature- or decision-levels.

Previous research on the registration in forests using mobile laser scanning (MLS) follows the dense data acquisition pattern (e.g., Qian et al., 2016; Kukko et al., 2017; Pierzchała et al., 2018; Shao et al., 2020; Hyyppä et al., 2020b; Balenović et al., 2021). The terrain-air registration, e.g., between TLS and Unmanned Aerial Vehicle (UAV) laser scanning (ULS), also belongs to the dense acquisition though the distance between viewpoints may be large. This is because the aerial view point covers a much larger area than the terrestrial view point which alleviates the low-overlap problem between viewpoints in the sparse acquisition, especially if the tie-features are used.

2.3.1. Data-level registration

Efforts toward data-level registration began shortly after TLS was first introduced in forests. Registration was performed with either Iterative Closest Point (ICP) or explicit tie-feature type of algorithms (Pfeifer and Briese, 2007).

Kelbe et al. (2016) proposed a pairwise registration method for the dense sensing mode, i.e., 25 scans at a grid pattern with 5-m baseline for a plot of 20 m × 20 m in size. The stem-terrain intersection points and the tree diameter at breast height (DBH) were used as tie features. The correspondences were found by an iterative RANdom SAmple Consensus (RANSAC) and a series of measures was applied to reduce the number of potential correspondences in order to overcome a prohibitive computational complexity and computational time in RANSAC. The global inconsistency in the pairwise registration has been a major challenge. The method was tested in 11 plots and evaluated by manually identifying true matches. The reported mean absolute errors were 7.8, 7.2, and 12.4 cm in translation along the *X*, *Y*, and *Z* axes, and were 0.93, 0.48, and 0.19 degrees in rotation angle around the three axes, respectively.

Tremblay and Béland (2018) used a similar idea as Kelbe et al. (2016) but replaced the geometric similarity by the lengths of the edges in a triangle, considering that the computation time increases quickly in scans with many trees detected. The test was made in five plots with five to eight scans in each plot. The average baseline ranged from 5.0 to 12.5 m. Each scan was matched to the closest scan. The deviation from reference registration parameters was calculated to evaluate the registration accuracy. The plot-level 3D translation errors ranged from 1.6 to 13.7 cm, and the average angular differences were between 0.0 and 16.1 mrad.

Liu et al. (2017) used stem curves, i.e., the stem diameters and centers at different stem heights, as features to derive the transformation parameters by minimizing the diameter differences and stem distance. The test was made in 10 forest plots of 32 m × 32 m in size. Five scans were made in each plot, and the baseline between the border and center scan was approximately 12 m. The horizontal *XY* and vertical *Z* translation root mean square errors (RMSE) were 1.63 and 13.14 cm, respectively, and the rotation RMSE was 4.38 min.

Dai et al. (2020) used crown modes as tie features to roughly find the overlap area and used the stem locations in the overlap area to build triangles to match point clouds. The test was carried out in the same 10 plots as in Liu et al. (2017). The mean horizontal and vertical translation errors were 1.13 and 7.21 cm, respectively, and the mean rotation error was 2.09 min.

Guan et al. (2020a) studied multi-platform lidar data registration in three study sites with stem density 283–1,056 trees·ha^{-1}. The triangulated irregular network (TIN) of 2D tree locations were used to find tree-pair correspondences. The following ICP registration applied ground points for a backpack-UAV registration and raw point clouds for a TLS registration. The backpack-UAV results were evaluated using a reflective plane. The errors were 14.6–30.0 cm in the two sites. The TLS results were evaluated by the standard deviation of residuals which were 3.8–5.3 cm in the third site.

Guan et al. (2020b) used features resembling rough ground points and rough tree stem locations for a coarse registration of scans, and ICP with raw point clouds for the fine registration. The method was tested in 6 plots with stem density 912–2,365 trees·ha^{-1} applying various scanning patterns, i.e., the baselines, number of scans and the scanning location patterns varied by data site. The accuracy was evaluated using the residual distance of artificial reference targets, and the errors were in the range of 2.4–6.8 cm. The method suffered from low overlaps between scans and for this reason the authors switched the reference scan for one target scan. The 2D registration method used an exhaustive search approach that resembles the one introduced in this paper, but it is less scalable due to a less efficient iteration strategy.

Zhang et al. (2021) used the fast point feature histogram (FPFH) method for the coarse alignment, ICP for the fine registration, and a graph-based global adjustment method. The method was tested in three plots with stem density 150–1,000 trees·ha^{-1} applying 4 or 5 terrestrial scans per plot and a single above-canopy UAV point cloud. The errors were evaluated using a different approach compared to what is commonly applied. Since artificial targets were not available in the evaluation, residuals of manually chosen corner features were reported instead, and the values were at the centimeter and meter levels after the fine and coarse registration, respectively.

Liu et al. (2021) matched ULS and TLS data using tree-height registration. The authors established correspondences for tree height points based on tree position and height similarities, and matched those points applying the least-squares method. ICP was used for the final registration. The method was tested in three plots with stem density 400–1,200 trees·ha^{-1} and the error evaluation was based on the average distance between the registered and reference registered point cloud data. The reported average accuracy was 0.43 m.

Additional information supports the registration. Henning and Radtke (2006) tried a pairwise registration method using wide-baseline point clouds, i.e., 15 scans with 10-m spacing for one plot of 20 m × 40 m in size. The method relies on the prior positions and angular orientations of the scanners recorded in the field to coarsely align range images. In a consequent study, Henning and Radtke (2008) matched three scans in the same forest plot in a leafless season. The baseline between one scan and its neighbor was 10 m and 14 m. The coarse alignment in the *XY* direction followed Henning and Radtke (2006). Both studies visually verified the registration accuracy. Bienert and Maas (2009) attempted to match two point clouds with 12-m baseline in one plot using automatically detected reference sphere and object distances. The study assumed the result to be sufficient for a coarse registration. Ni et al. (2011) used the inclinometer to measure the rotation angle around the *X* and *Y* axes, and field-measured scanner distances in the *X* and *Y* directions to support the search for corresponding points. The test was made in one pine plot of approximately 40 m × 40 m in size using five scans. The difference between registration results and total station measurements was used to evaluate the horizontal and vertical registration errors. The mean *X*, *Y* and *Z* errors were 2.1, 1.8 and 7.6 cm, with ranges 0.3–4.5, 1.1–2.4 and 1.5–22 cm, respectively. Hilker et al. (2012) used four spheres as targets to determine the pairwise registration between the border and center scans. The sphere locations were approximated using field-measured distance and bearing, and the spheres were extracted from the TLS data according to the laser intensity. The test was made in five 30 m × 30 m plots. The registration results were evaluated by the quality of the terrain extracted from the combined TLS data set. Zhang et al. (2016) used a flat circular reflector beneath the TLS scanner in the pairwise registration. The reflector coordinates were determined by the distance between the reflector and the scanner measured by a steel tape, and were used to estimate the three translation parameters. The rotation angles were obtained from the scanner inclination sensor and digital compass. The test was performed in two 45 m × 45 m plots, using 10 and 14 scans, respectively. The registration accuracy was approximately 1.5 cm. Paris et al. (2017) used GNSS and nominal orientation measurements at each scan location as the initial position estimates, and minimized the difference between normalized canopy height models from TLS and ALS to link TLSs in non-overlapped open forests. Conventional accuracy parameters were not reported. Guan et al. (2020a) assumed that every forest stand has a unique spatial tree pattern. Measures such as the area and angle between TIN triangles were used to find similar triangles, and position pairs were refined by RANSAC. Point clouds from two sources were further matched using ICP based on either ground or trunk points. The experiment was carried out in three plots, i.e., 283, 275, and 1,056 trees·ha^{-1}, and the evaluation was based on the point-plane distance and standard deviation in the MLS-ULS and TLS cases, respectively.

2.3.2. Feature- and decision-level registration

Other than the direct registration of a set of point clouds and merging all point clouds, the matching can be carried out at feature- and decision-levels. Liang and Hyyppä (2013) proposed a feature- and decision-level registration method. Stem features were extracted from each point cloud and the registration was carried out using the preliminary stem locations.

Methods of this type have a lower computational complexity than data-level registration methods. They can be directly applied to multiple platforms, e.g., terrestrial and mobile mapping systems (Liang et al., 2018b; Polewski et al., 2019), can solve the problem associated with the wind where trees may sway in the merged point cloud, and provide solutions to merge point clouds from different data sources (Mulverhill et al., 2020).

The features used are mostly tree positions (Liang et al., 2018b; Polewski et al., 2019; Mulverhill et al., 2020), and the combination of several attributes, e.g., the tree position and top (Liu et al., 2021).

Polewski et al. (2019) registered UAV and backpack lidar point cloud by first aligning the *Z*-axes of the point clouds by computing the median tree growth directions based on stem models. The potential corresponding tree pairs were found by solving a maximum-weight matching of a bipartite graph of trees where the weights were given by a similarity measure based on the distributions of inter-tree distances. The optimal tie points were selected using a modified RANSAC-style criterion. The method was tested in 7 plots with stem density 242–744 trees·ha^{-1}, and the mean position deviation of trees was 27–67 cm.

The challenge of this type of methods lies in the decision making, i.e., how to select an estimate among those that are not fully recorded in individual data sets. Similar to the data-level registration, the limited feature availability is another possible limitation. Liu et al. (2021) noticed that the lack of crown data in TLS represents the main cause of the registration errors.

3. Materials

The test field and the data used in this study are briefly introduced in Sections 3.1–3.3. More details about the field and data can be found in Liang et al. (2018a, 2019). The collection of the reference data, i.e., the positions of the artificial targets set up in the sample plots, is detailed in Section 3.4, where the sphere positions before and after the transformation serve as the evaluation criterion.

3.1. Test sites

The test site is located at Evo, Finland (61.19° N, 25.11° E). The area comprises varying boreal forest types with variable species compositions, growth stages and management history. The main tree species are Scots pine (*Pinus sylvestris* L.), Norway spruce (*Picea abies* (H. Karst) L.), Silver birch (*Betula pendula* Roth) and Downy birch (*Betula pubescens* Ehrh.).

The test data covered 24 forest sample plots of 32 m × 32 m size. The forest stands represent diverse boreal forest stand conditions and, thus, represent different difficulty levels of data processing, i.e., feature extraction and point cloud registration. They were classified into three stand complexity categories with respect to the in situ visibility, the stem density, and the DBH distribution. The ground level visibility notably decreased from the easy to the difficult category, which significantly affected the TLS line-of-sight. Also, the reliability of the forest attribute estimates steadily decreased as the forest conditions became more complicated (Liang et al., 2018a).

All trees inside the sample plots with DBH >5 cm were recorded, and their DBH and tree height were measured with calipers and Vertex III digital inclinometer (Haglöf AB, Sweden), respectively. Fig. 1 illustrates the TLS center scan point clouds of the example plots in each complexity category, to illustrate the forest conditions involved in this study. Table 2 summarizes the field-measured plot-level statistics averaged according to the stand complexity categories. With the increase in stand complexity,

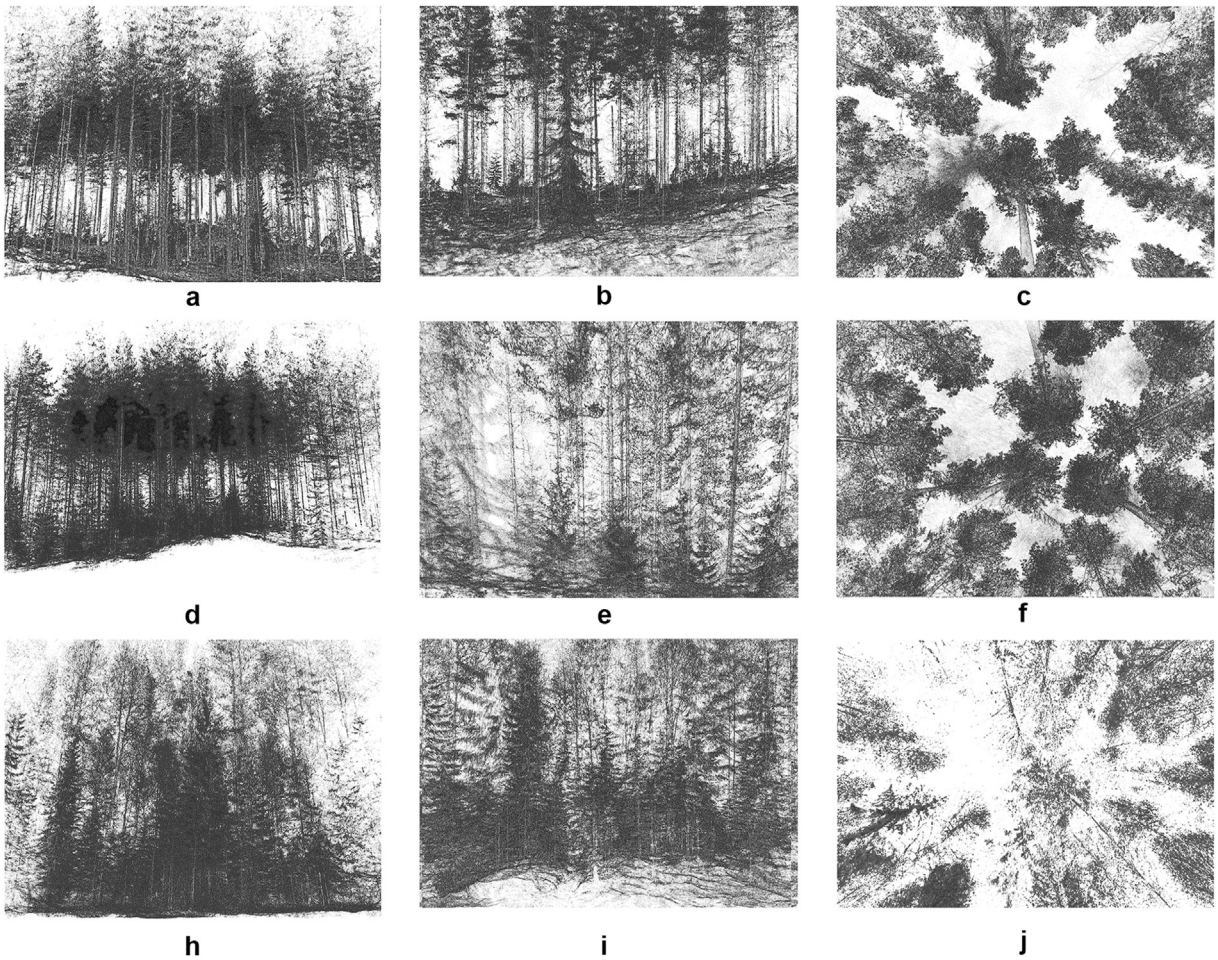

Fig. 1. Examples of forest plots in terrestrial data from different complexity categories. (a–c), an easy plot dominated by Scots pine with minimal understory and good line-of-sight. (d–f), a medium plot dominated by Norway spruce with more understory and a decreased line-of-sight near the forest floor, (h–j), a complicated plot of mixed species with dense understory and severely limited line-of-sight both near the floor and toward the canopy. (a, d, h) and (b, e, i) illustrate the horizontal views from outside and inside the plot, respectively. (c, f, j) illustrate the bottom-to-top views.

Table 2
Summary of the properties of the 24 sample plots used in this study in three complexity categories, i.e., the understory vegetation density, species composition (pure, or mixed), mean and standard deviation values of diameter at the breast height (DBH), basal area, tree height and the stem density.

Complexity categories	Understory vegetation	Species composition	DBH (cm)	Height (m)	Basal area ($m^2 \cdot ha^{-1}$)	Stem density ($trees \cdot ha^{-1}$)	Number of plots
Easy	Minimal	Pure	20.7 ± 8.5	18.4 ± 6.4	23.2 ± 5.9	592 ± 189	7
Medium	Sparse	Pure/Mixed	17.2 ± 10.7	16.2 ± 7.3	31.2 ± 8.6	968 ± 370	9
Difficult	Dense	Mixed	12.3 ± 7.2	13.2 ± 5.9	32.3 ± 7.1	2021 ± 553	8

the stem density increased, and the mean values of DBH and tree height decreased. This indicated a rising amount of small and young trees within a plot which consequently increased the occlusion effects.

3.2. In situ TLS data acquisition

The sample plots were scanned in 2014 using a Leica HDS6100 (Leica Geosystems AG, Heerbrugg, Switzerland) TLS scanner, using a multi-scan TLS approach. Five scans were made in each plot, i.e., one scan at the plot center and four scans at the four quadrant directions. The targeted distance between the border and center scan was 11.3 m, but varied depending on the plot conditions. In practice, the scanner should be placed sufficiently far away from nearby trees and bushes to avoid substantial occlusion, which sets restrictions for the scanner locations.

Fig. 2 illustrates the scan-to-scan distances for each center-border scan pair and their plot-wise averages in each of the 24 plots. The average a distance in each plot were approximately 10 m, i.e., the average distance over easy, medium and difficult plots were 10.2, 9.9 and 8.7 m, respectively. The mean scan distance at the plot level ranged from 7.9 to 11.4 m, while the range at scan-level was from 6.3 to 13.3 m. Nine of the border scans had a distance less than 7.5 m, two of which were in easy plots, two in medium plots and five in difficult plots. The realized scan distances fell short of the target value due to limited visibility and feasible scanning locations.

The plots were scanned as they were, i.e., without any pre-scan preparation operations such as removing lower vegetation or branches before the TLS data collection. The scanner gave a 1.57-cm horizontal and vertical point distance and ±2 mm distance measurement accuracy at 25-m distance from the scanner.

Six artificial spherical reference targets with a known radius were

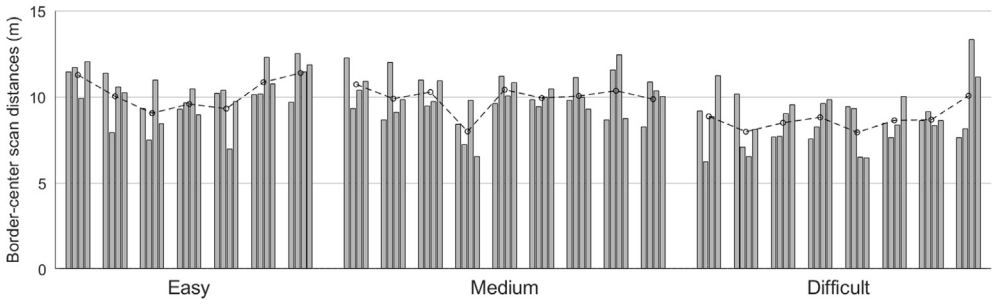

Fig. 2. Center-border scan distances for each of the 24 plots of three complexity categories. Each bar represents a border scan, and each plot has 4 bars. The height of a bar presents the distance between the center and border scanning locations in *XYZ* space, which was computed based on the reference registration parameters. The average scan distances over the plots are depicted by the circles.

Table 3
The sphere fit statistics over all targets in all plots and scans given as minimum, 1st (Q_1), 2nd (Q_2), and 3rd (Q_3) quartiles, maximum and mean RMSE in millimeters.

	Min	Q_1	Q_2	Q_3	Max	Mean
RMSE (mm)	0.62	1.49	1.78	1.86	2.68	1.66

placed within each plot to enable co-registration. The targets were placed such that all six spheres were visible in the center scan, and at least three spheres were visible in each border scan.

3.3. Unmanned aerial vehicle (UAV) data acquisition

The UAV-borne LS (ULS) data were collected over the same area as the TLS dataset. In total, 22 plots of the previously mentioned 24 plots were scanned in September 2017 using a Riegl RiCOPTER (RIEGL, Horn, Lower Austria, Austria) with a Riegl VUX-1UAV scanner. Both the UAV platform and the onboard sensors are high-end systems that represent the current highest quality UAV data. The geometric accuracy of the aerial UAV data is, however, lower than that of the static TLS.

The flight altitude was approximately 50 m above the ground, with a typical flight speed of 2.0–4.0 m·s^{-1}. Each plot was covered with 4–5 overlapping flight lines and the resulting point density was 4,000–18,000 points·m^{-2} at the sample plot areas.

The GNSS-IMU system on the drone measures the platform position with 0.1-m horizontal and 0.2-m vertical accuracy. The measurement errors in roll, pitch and heading were within 0.015, 0.015 and 0.035 degrees, respectively. These gave a point location accuracy within 3.6 cm at the nadir and 7.1 cm at the far end of the field-of-view at 50-m altitude, when the positioning and ranging errors are not considered.

The visibility of trees varied significantly according to tree species and forest structure, as shown in the Fig. 5 in Liang et al. (2019). Pine trees in easy forest stands typically had an excellent visibility. Spruce trees, and especially their stems, can be either partly visible or completely occluded by their own canopy and/or by canopies of the surrounding trees.

3.4. Reference data for evaluation

The target positions in each individual scan were first manually located from the point clouds, and were further refined with an automated least-squares approximation to acquire reliable reference data for evaluating the automated registration results. All spheres with more than 1/4 of the sphere surface covered in the point clouds were used as reference targets.

The refinement eliminated erroneous laser points that were close to the spheres but did not strictly correspond to the sphere surface, e.g., due to the measurement. Points around the sphere close enough to the estimated sphere surface were selected, and the deviations between the sphere radius and the points' distance to the sphere center were minimized to find the refined center using a least squares approach. The reference registration parameters were computed from the corresponding targets.

Table 3 reports the statistics over all targets in all plots and scans. The mean $RMSE_{\text{sphere}}$ over all the targets was 1.66 mm, and the mean plot-wise and scan-wise reference registration errors were both 1.90 mm. Fig. 3 reports the reference registration errors in individual plots and scans in *XYZ*, *XY* and *Z*. The *RMSE* was defined as $RMSE = \sqrt{\frac{1}{N}\sum_{i=1}^{N}\left\|c_i^C - f(c_i^B)\right\|^2}$, where f is the reference transformation while c^C and c^B are the sphere centers in the center and border point clouds, respectively. The contributions of *XY* and *Z* space errors to *XYZ* space errors were estimated by the ratios r_{XY} and r_Z as defined in Eqs. 2 and 3.

$$r_{XY} = RMSE_{XY} \,/\, (RMSE_{XY} + RMSE_Z) \tag{2}$$

$$r_Z = RMSE_Z \,/\, (RMSE_{XY} + RMSE_Z) \tag{3}$$

According to Fig. 3, no significant difference in the reference registration parameters' accuracy between the complexity categories was observed.

4. The proposed registration algorithm

This section first overviews the proposed method, and then details the proposed algorithm in Sections 4.2 to 4.6, namely, the automated feature point extraction, initial registration, fine registration, multi-dataset registration, global registration, and the evaluation methods. It should be noted that the proposed method does not apply the artificial reference targets in any way. The reference targets are solely used for evaluation purposes.

Throughout the rest of the paper, the two point clouds considered in the matching are referred to as the reference and target. The registration aims to find a rigid mapping $f : R^3 \rightarrow R^3$ to transfer the target to the coordinate system defined by the reference.

4.1. An overview of the registration method

Wide-baseline observations in forest conditions are characterized by the deficient overlap between observations, self-similar structures, and the lack of external information, which may mislead the registration to converge to a local optimum. This study proposes a point-cloud registration algorithm through an initial alignment at the feature level followed by a precise fine registration at the data level. The initial registration reconstructs the rough geometries between wide-baseline observations with high noise level by solving the six degrees of freedom (DoF) problem with unknowns $\{X, Y, Z, yaw, pitch, roll\}$ in two consecutive steps in lower dimensions. The fine registration searches and analyzes overlap points that are covered by both point clouds and derives the 6 DoF registration parameters.

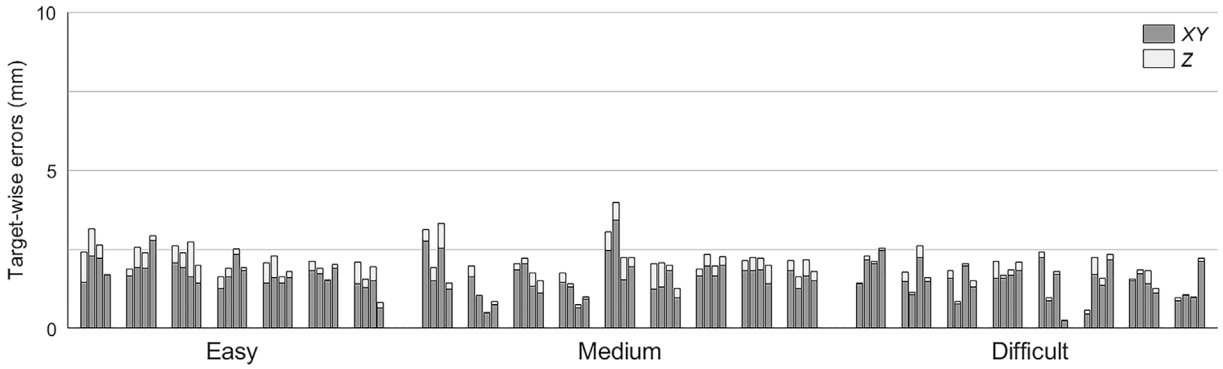

Fig. 3. Target-wise reference registration errors for each target point cloud in 24 plots in three complexity categories. Each bar represents a center-border point cloud pair, and each plot has 4 bars. The total height of a bar represents the *RMSE* in *XYZ* space from the common target positions between the center and border point clouds when the reference registration parameters are applied. In each bar, the bottom (gray) and top (white) parts represent the ratios r_{XY} and r_Z of the errors in *XY* and *Z* directions to the total amount of errors, respectively.

More specifically, this study proposes a new framework for finding correspondences to solve the problem of deficient overlap between point clouds. The DOS method uses space discretization to represent the target and reference point clouds, and applies matrix operations to find correspondences with high confidence. This study also proposes a deterministic 2D registration method as an alternative to popular sampling-based methods, which seems to be more stable and robust than the sampling-based methods.

The registration uses an accumulative concept such that the reference scan grows step by step as the matched target scans are added to the reference scan. The expanded reference scan increases the data coverage over observed objects and increases the overlap area between the reference and the remaining target scans. Thus, theoretically, the probability of a successful registration increases along with the growth of the reference scan. In addition, a global matching is adopted to study the error accumulation in the method. In this paper, the global matching is presented as an optional step as, according to our experiment, it may not be strictly necessary for achieving highly accurate results.

Fig. 4 illustrates the flow chart of the proposed method.

4.2. Automated retrieval of feature points in forest environments

Reconstructing the geometry between the reference and the target point clouds relies on the existence of common points in both point clouds. Three types of feature and object points were used as common points, namely, the stem positions, the stem points, and the ground points.

The ground points were detected using a morphological filter. The point cloud was first rasterized in 2D with a 20-cm section size. The lowest point in each 2D section was used as a seed point and the largest connected group was considered to be part of the ground. Detached groups were added to the ground if they were smoothly connected with the accepted ground.

Stem points were identified by a point distribution analysis which allowed finding points that have a vertical and flat distribution in their immediate neighborhood. Tree-stem models were built from the recognized stem points as a series of 3D cylinders representing the changes in the stem growth direction. The stem locations were extracted from the cylinder positions at the 1.3-m height as commonly used in forest applications. For more details about the extraction of ground and stem

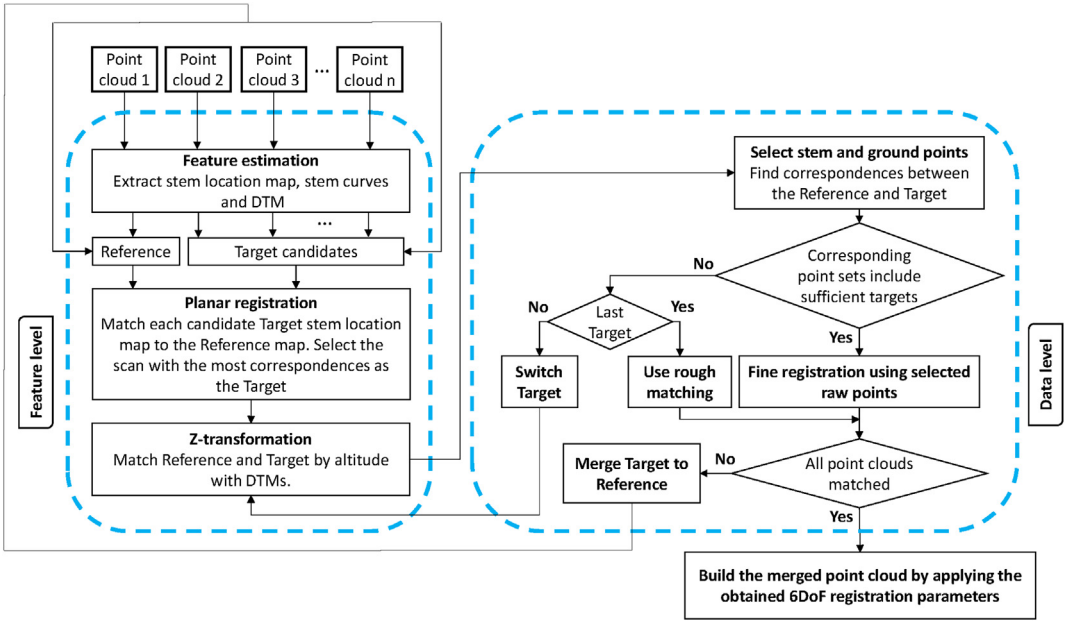

Fig. 4. The flow chart of the method.

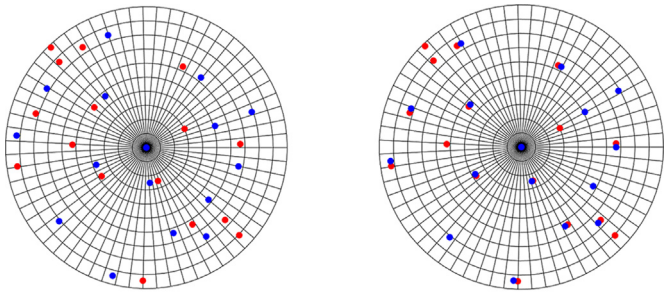

Fig. 5. An illustration of the 2D-registration idea. The red and blue points represent the points in point sets A and B, respectively. The center of the circle shows the current aligned pair (a_i, b_j) and the sections represent the discretization. (a) shows a correct point pair (a_k, b_k) with an incorrect rotation, while (b) shows the same scenario with a two-step rotation of B in the anticlockwise direction. The number of correspondences between point sets A and B is found as the number of point pairs located within common sections. (For interpretation of the references to color in this figure legend, the reader is referred to the Web version of this article.)

points, as well as modeling the stems, the reader is referred to Liang et al. (2018b).

4.3. Initial registration

The initial registration aims to reconstruct the relative position and orientation between observations and approximately transfers the target data to the reference coordinate system. The initial alignment relies on the extracted feature points. The 6 DoF registration problem was solved in three separate steps in lower dimensions. In the state-of-the-art hardware setup, the scanner is leveled during the data acquisition, so that *pitch* and *roll* angles are small. The 6 DoF registration can thus be modeled as three separate registration problems in two dimensions (2D) with 3 DoF $\{X, Y, yaw\}$, in one dimension with 1 DoF $\{Z\}$, and in 3D with 2 DoF $\{pitch, roll\}$, respectively. Since *pitch* and *roll* are approximately zero, the initial registration is practically solved by a planar and vertical registration.

4.3.1. Planar registration

Given two point sets $A = \{a_i\}_{i=1}^{M} \subset R^2$ and $B = \{b_i\}_{i=1}^{N} \subset R^2$ defined by two stem location maps from the reference and target point clouds, respectively, let a set of matched points between them be $\{(a_k, b_k)\}_{k=1}^{L}$. Let $\mathscr{T} = \{R_\theta, t\}$ be a rigid transformation matching the two point sets, where R_θ is a rotation matrix defined by a rotation angle θ and t is a translation vector so that $a_k = R_\theta b_k + t + \varepsilon_k$, where ε_k is an error vector. The planar registration aims to find the best corresponding points (a_k, b_k) and rotation angle θ, which define $\mathscr{T} = \{R_\theta, t\}$ where $t = a_k - R_\theta b_k$.

Without any external information, the transformation $\mathscr{T}$ between A and B was found by iterating over the point pairs and rotation angles and by finding the best matches. The sets were aligned with respect to each pair (a_i, b_j), the target set B was rotated around b_j with rotation angles $\theta \in [0, 2\pi)$, and the set of matching points between A and B was estimated.

The 2D geometry was reconstructed through a space discretization searching mechanism. The area surrounding the current points (a_i, b_j) with radius Rad was discretized in distance and angle directions into $n_P = ceil(Rad/d)$ and $m_P = ceil(2\pi Rad/d)$ sections, respectively. The discretized space was represented as an $n_P \times m_P$ binary matrix B, where each section corresponds to an entry of the matrix and the entry had a value 1 if it was occupied by at least one tree, and a value 0 otherwise.

Thus, the correspondences between two spaces could be found by the Frobenius inner product of the reference matrix B_R and target matrix B_T

$$\langle B_R, B_T \rangle = \sum_{i=1}^{n_P} \sum_{j=1}^{m_P} (B_R)_{ij} (B_T)_{ij} \tag{4}$$

and the rotation with respect to b_j is given by the matrix column shift operation

$$f_l : [c_1, c_2, \ldots c_{m_P}] \mapsto [c_{m_P - l + 1}, \ldots, c_{m_P}, c_1, \ldots, c_{m_P - l}] \tag{5}$$

where $B = [c_1, c_2, \ldots c_{m_P}], c_j \in R^{n_P}$ and $l \in [1, m_P)$ is the rotation parameter which corresponds to a rotation $\theta_l = 2\pi l / m_P$. The score $C_{ij}^l \in [0, L)$ for all correspondences between A and B with respect to the current pair (a_i, b_j) under rotation θ_l is thus given by $C_{ij}^l = \langle B_R, f_l(B_T) \rangle$.

The idea of the 2D matching is illustrated in Fig. 5.

Since matching points may be located in nearby or neighboring sections, a filter is applied to the reference matrix B_R. This results in $3d \times 3d$ buffer zones around each point in the reference point set A, which essentially defines a distance threshold in finding the matching points.

The searching process composed of an iteration over all point pairs and was followed by a hierarchical selection of the best combination of point pair and rotation, aiming to avoid the selection of a local optimum, and a least square refinement.

The 2D matching workflow is described as follows:

for each tree a_i in Reference scan
  for each tree b_j in Target scan
    • Align scans with respect to trees a_i and b_j
    • Find matrices B_R and B_T, and apply filter K to B_R
    for each rotation of angle θ_l for Target scan with respect to b_j
      • Compute score $C_{ij}^l = \langle B_R, f_l(B_T) \rangle$
    end for
  end for
end for
• Sort the results according to C_{ij}^l
• Select the best θ_l and (a_i, b_j)
• Refine the matching to acquire the final transformation $\mathscr{T}$

4.3.2. Z-transformation

The preliminary 2D registration recovers the $\{X, Y, yaw\}$. The unknown shift in the Z direction was retrieved by matching two digital terrain models (DTM). The DTM from the target scan was transferred into the reference scan coordinate system using the transformation $\mathscr{T}$. For each point in the DTM of the target scan, its closest planar counterpart of the reference DTM was found, and the Z transformation was retrieved as the Z direction shift that minimized the vertical RMSE between two DTMs.

Given two DTMs $C, D \subset R^3$, let the subsets of nearest planar neighbor points be denoted by $C_Z = \{c_i\}_{i=1}^{M}$ and $D_Z = \{d_i\}_{i=1}^{M}$, and the points satisfy $\| (d_i)_{XY} - (c_i)_{XY} \| \leq \varepsilon$ where $\varepsilon = 0.1$ m. The vertical RMSE of the corresponding points is

$$RMSE(\mathscr{C}_Z, \mathscr{D}_Z) = \sqrt{\frac{1}{M} \sum_{i=1}^{M} \left| (c_i)_Z - (d_i)_Z \right|^2} \tag{6}$$

and the Z-transformation is given by $\underset{x \in (-\infty, +\infty)}{\operatorname{argmin}} RMSE(\mathscr{C}_Z, \mathscr{D}_Z + x)$.

4.4. Fine registration

The main challenges in the data level registration are the low overlap and the structure outlier problems that can mislead the registration to converge to a local optimum. With the rough geometry information between point clouds retrieved in the initial transformation step, the fine registration approach aimed to select points that potentially have correspondences between point cloud pairs and to fine-tune the registration. The overlap selection methods follow the same general DOS framework that was employed in the planar registration.

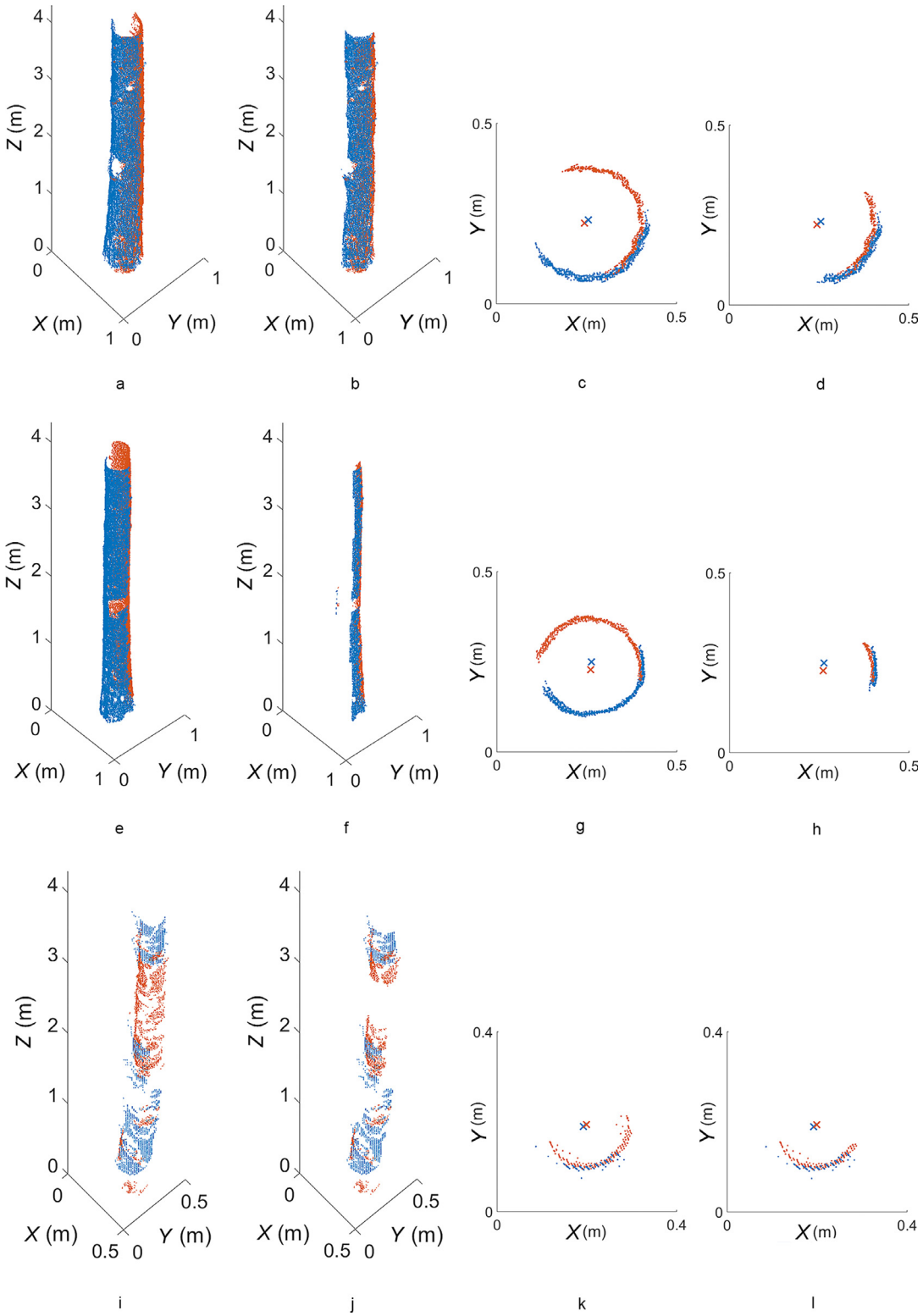

Fig. 6. The stem point selection procedure for finding the correspondence area between scans. Stem points in (a–d), (e–h), and (i–l) correspond to three individual trees in the TLS point clouds after initial registration. The points in each group are from the same tree in 3D and 2D. The stem points in the reference and target scans are in blue and orange, respectively. All points are in the reference coordinate system after the initial registration. The points in 2D are from a 20-cm section in the *Z* direction and projected onto the *XY* plane, and the crosses of corresponding colors are the estimated tree centers. (a, e, i) illustrate the stem points from both the reference and target scan aligned in the reference coordinate system. (b, f, j) illustrate the selected potentially overlapping stem points from both the reference and target scans. (c, g, k) illustrate the complete stem points in the reference and target scans in 2D in the *XY* plane. (d, h, l) illustrate the selected, potentially overlapping stem points from reference and target scan in 2D in the *XY* plane. (For interpretation of the references to color in this figure legend, the reader is referred to the Web version of this article.)

4.4.1. Tree-stem point selection

Given the rough geometry recovered by the initial registration, common tree pairs (a_k, b_k) were analyzed to identify the overlapping stem points between the two point clouds.

3D stem points (x, y, z) in each individual tree of a common tree pair (a_k, b_k) were discretized into n_S and m_S altitude- and angle-wise sections according to their altitude Z and observation angle φ defined with respect to the stem center estimates. Here $n_S = ceil((Z_{max} - Z_{min})/Z_{stp})$ and $m_S = ceil(2\pi/\varphi_{stp})$, where Z_{max} and Z_{min} are the maximum and minimum altitudes Z of the tree-stem points and Z_{stp} and φ_{stp} are the altitude and angle discretization step sizes. The step sizes 0.1 rad and 0.1 m are expected to correspond to the errors in the stem curve estimation and in the initial registration in the Z direction in the sense that the reference and target coordinates should satisfy $|Z_T - Z_R| \leq 2Z_{stp}$ and $|\varphi_T - \varphi_R| \leq 2\varphi_{stp}$. Considering the wind effects that may lead to tree swaying, only stem points at low altitudes between the stump and $H_S = 4$ m height were considered, since the stems are typically stiff and their movements in windy conditions are correspondingly minor.

Given the discretization, the overlapping 3D stem points in the reference and target were found in a similar way as in the planar registration using DOS. Among all trees having overlap between point clouds, the stems with the best visibility were selected. The trees were ranked according to the score S_N, i.e., $S_N = N_R N_T$ where N_R and N_T are the numbers of selected stem points in the reference and target point clouds, respectively. A high S_N score indicates a good stem visibility in both point sets simultaneously. N trees with the highest S_N score were selected, and N equaled 20.

Fig. 6 illustrates the proposed method for the tree-stem point selection. The three rows illustrate three cases with varying stem visibility. The first row shows a tree that has considerable overlap between two point clouds. The second row is a tree that has barely any overlap between point clouds since it stands in the middle of two scans. The third row is a tree under heavy occlusion, where the overlap area is much smaller than that without occlusion. The point distribution analysis identified points with potential correspondences in the other scan. It removed non-overlapping points to reduce the outliers in the registration, as illustrated in the second and fourth row in the figure.

4.4.2. Ground point selection

In order to improve the registration accuracy, the method considered ground points simultaneously with the stem points. Tree stems are self-similar structures, especially in the vertical growing direction, which makes stems less reliable for registration and is one of the main reasons for the commonly large Z-direction registration error in previous reported studies. Altogether, the wide-spread stem and ground points helped to relieve the self-similarity problem in the wide-baseline point cloud registration.

The forest floor is noisy because it is full of shrubs, stones, stumps, and dead branches/stems. Algorithms for detecting ground points in general work well but errors are still present (Liang et al., 2018b), namely, some object points might remain in the classified ground points. In the registration, bare ground points are preferred, since their correspondences in other scans, if such exist, are less affected by the changing viewing geometries than other objects such as stones and shrubs.

To find common ground points between datasets, the rectangular area delimiting both reference and target ground points was discretized into n_G and m_G sections with resolution d concerning x and y coordinates, respectively. A section was considered if at least $N_G = 20$ ground points existed within. The resolution d corresponds to the tolerance of the 2D matching in the initial registration so that the possible correspondences between reference and target data sets can be found even if the 2D matching in the initial registration was only rough. The overlapping ground points in the reference and target scans were found using DOS, similar to what was done in the planar registration. Fig. 7 illustrates the ground point distributions of two neighboring scans and the selected common ground points.

4.4.3. Fine registration

After retrieving potential correspondences, ICP algorithm was applied to the selected reference and target points given by sets C and D, respectively, to improve the initial registration. ICP attempts to find iteratively the rotation $\mathscr{R}$ and translation $\mathscr{t}$ that minimize the average of the squared errors of corresponding points $c_i \in C$ and $d_i \in D$ given by

$$E(\mathscr{R}, \mathscr{t}) = \frac{1}{m}\sum_{i=1}^{m} \|c_i - \mathscr{R}d_i - \mathscr{t}\|^2 \quad (7)$$

The sets of corresponding points $C_N \subset C$, $D_N \subset D$ considered at each iteration consisted of those points c_i and their closest counterparts d_i in D for which $\|c_i - d_i\| \leq \varepsilon$. In this study, ICP was applied consecutively with two criteria, i.e., $\varepsilon_1 = 0.10$ m and $\varepsilon_2 = 0.03$ m.

4.5. Multi-dataset registration

Sections 4.3 and 4.4 outlined the registration of two individual scans. The proposed registration method takes an accumulative strategy where

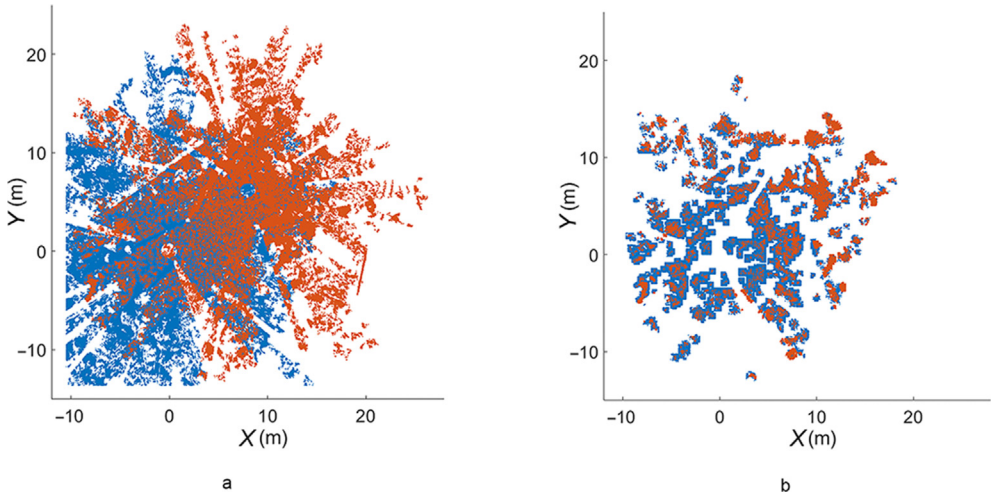

Fig. 7. Ground points in two exemplary point clouds (a) before and (b) after the ground point filtering. The blue and orange points represent the reference and target scans, respectively. (For interpretation of the references to color in this figure legend, the reader is referred to the Web version of this article.)

the reference scan grows by adding the matched target scans to the reference scan.

In a sparse data-acquisition setup, the point cloud at the center is used as the initial reference scan. The next target point cloud was selected as the unmatched scan with the highest number of correspondences according to the 2D registration. When a target point cloud was matched with the reference, the two stem location maps were merged to build a new enlarged reference map. The matching trees in the two stem location maps were merged if they were within a distance of $2d$. The average of these two positions was the new tree position. The point clouds were concatenated to cover the whole space. A detailed workflow is described as follows:

```
• Assign the center point cloud as the Reference
for each matching
  for remaining point clouds
    • Perform planar registration with the Reference
  end for
  • Sort point clouds by correspondences in descending order
  for sorted scans
    • Assign the next point cloud as the Target
    • Find Z-transformation to match the Target with the Reference
    • Find overlapping ground and stem points
    if sufficient targets are selected
      • Match selected points from the Target and the Reference with ICP
      • break
    else
      if all Target have been considered
        • Use initial registration parameters
      end if
    end if
  end for
  • Merge matched Target and Reference
end for
```

4.6. Global registration

In general, the registration errors are expected to accumulate in accumulative registration approaches. In this study, the (optional) global registration step is performed using the multi-view extension to the ICP algorithm (Pooja and Govindu, 2010) which is based on the Lie-algebraic averaging method (Govindu, 2004). It relies on averaging pair-wise registration results over closed mapping loops.

Let $M_{ij} = \begin{bmatrix} R_{ij} & t_{ij} \\ 0 & 1 \end{bmatrix}$ be the mapping in homogeneous coordinates taking scan i from its local coordinate system to the local coordinate system of scan j. The Lie algebraic global registration minimizes the violations in the so-called consistency equations $M_{j1}M_{ij}M_{i1}^{-1} = I$ which state that the composition mappings corresponding to closed mapping loops should equal to identity. The averaging is achieved by an iterative scheme resembling gradient descent. That is, incremental improvements to the mappings are made by projecting the equations from the special Euclidean group $SE(3)$ to its Lie algebra $se(3)$, and back, using the matrix exponential and logarithm functions. For details, the reader is referred to the original papers.

The multi-view ICP algorithm comprises the correspondence, motion estimation and averaging steps, which are repeated iteratively. That is, at each iteration, the overlap is found for each pair of neighboring scans using the DOS method, and the pairs with sufficient overlap are selected. The nearest neighboring points between the scans are found and the corresponding optimal adjustments are computed. The adjustments are applied to the registration parameters, and the motion averaging algorithm is applied to find globally consistent registration parameters for the target scans.

Table 4
A summary of the descriptions and values of the parameters used in the method.

Parameter	Description	Value	Unit
d	Expected uncertainty level in 2D point sets	0.2	m
H_S	Stem height considered to eliminate the wind effects	4.0	m
Z_{stp}	Altitude-wise discretization parameter in the stem point filtering	0.1	m
φ_{stp}	Angle-wise discretization parameter in the stem point filtering	0.1	rad
N_G	The minimum number of ground points in each section	20	–
ε_1	Criterion on the first round of ICP	0.1	m
ε_2	Criterion on the second round of ICP	0.03	m

4.7. Evaluation

4.7.1. Accuracy of terrestrial point clouds

The registration accuracy was evaluated using three quantitative criteria: 1) the 3D distance between the sphere centers of the artificial reference targets in the center scan and the corresponding sphere centers in border scans after applying the derived registration parameters, i.e., target-wise transformation errors, 2) the difference in the six transformation parameters between the reference parameters calculated from the reference targets and their counterparts obtained from the registration algorithm, and 3) a theoretical error upper bound for the point-wise difference between the reference and algorithm-derived transfer parameters.

Given the algorithm-derived registration parameters (R, t), the distances between the target sphere centers c^R in the reference data set and the corresponding target centers in the transformed target data set $f(c^T, R, t)$ provide a quantitative evaluation of the registration accuracy. The registration parameters were derived from both the proposed registration algorithm and the reference sphere center coordinates to obtain the algorithm-derived parameters (R, t) and the reference parameters (R_r, t_r). Accordingly, both the algorithm- and reference-target-based $RMSE_{XYZ}$ values were reported. While the algorithm-related $RMSE_{XYZ}$ evaluates the accuracy of the proposed method, the reference-target-related $RMSE_{XYZ}$ values, presented in Fig. 3 in Section 3.3., express the data-level errors associated with the hardware and data acquisition. Furthermore, the contributions of XY and Z space errors to XYZ space errors were estimated by r_{XY} and r_Z ratios, as defined in Section 3.3.

The parameter-level evaluation compares the 6 DoF algorithm-derived (R, t) and reference registration parameters (R_r, t_r). The difference was reported in translations including X, Y, Z, XY and XYZ, and in rotations *yaw*, *pitch*, and *roll*.

The theoretical upper bound defined by Eq. 8 was calculated in order to estimate the maximum point-wise difference between parameters (R, t) and (R_r, t_r) within a distance $\|p\|_2$ from the target scanning position.

$$\|R_r p + t_r - (Rp + t)\|_2 \leq \|R_r - R\|_2 \, \|p\|_2 + \|t_r - t\|_2 \tag{8}$$

With the upper bound, the difference at 5 and 10 m was estimated for each matched target scan by finding the scan-wise values for $\|R_r - R\|_2$ and $\|t_r - t\|_2$.

4.7.2. Stability of terrestrial point clouds

The stability of the proposed method was primarily evaluated in the study by the varying forest complexity conditions. In addition, the stability was evaluated by examining the parameter sensitivity of the results. The method's parameters, summarized in Table 4, were increased and decreased by 5%, 15%, and 25% of the values introduced in the methods section.

Given the five point clouds in each sample plot, there were four target-reference registrations for the generation of an integrated point cloud. For each registration, six new registration results were calculated using modified parameter values and in total 576 new matches with new

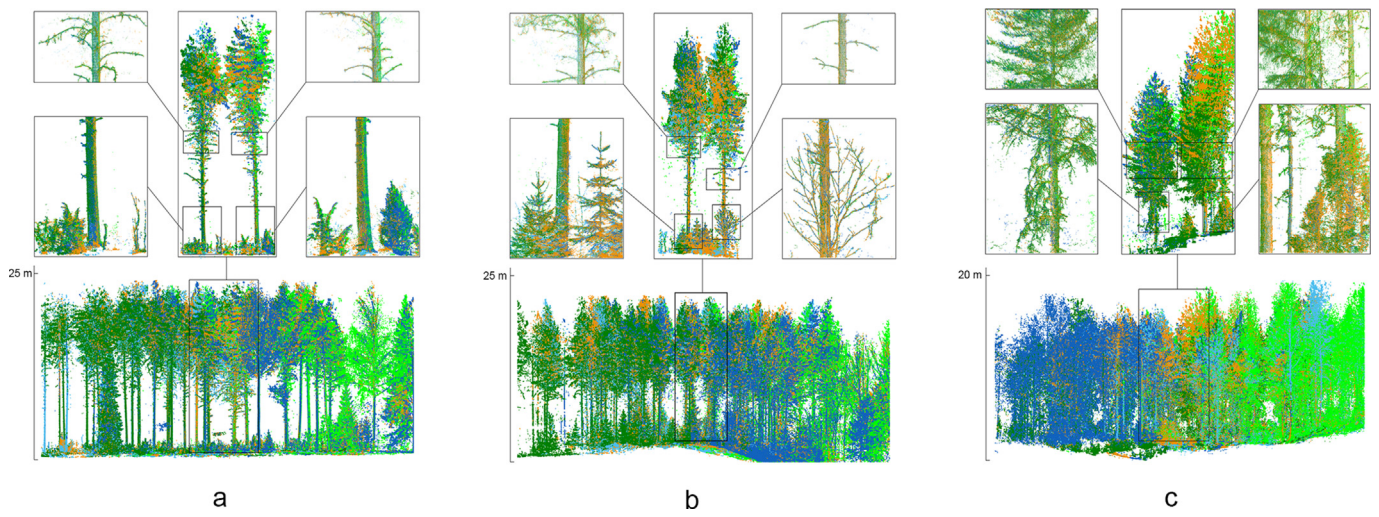

Fig. 8. An illustration of the registration result acquired from the proposed algorithm in (a) easy, (b) medium and (c) difficult plots. Each color represents one of the five scans in the merged point cloud. The bottom figure shows a horizontal view of a planar subsection of the plot. Close ups are shown for mature trees in the plot and some bushes or young trees in their close proximity. (For interpretation of the references to color in this figure legend, the reader is referred to the Web version of this article.)

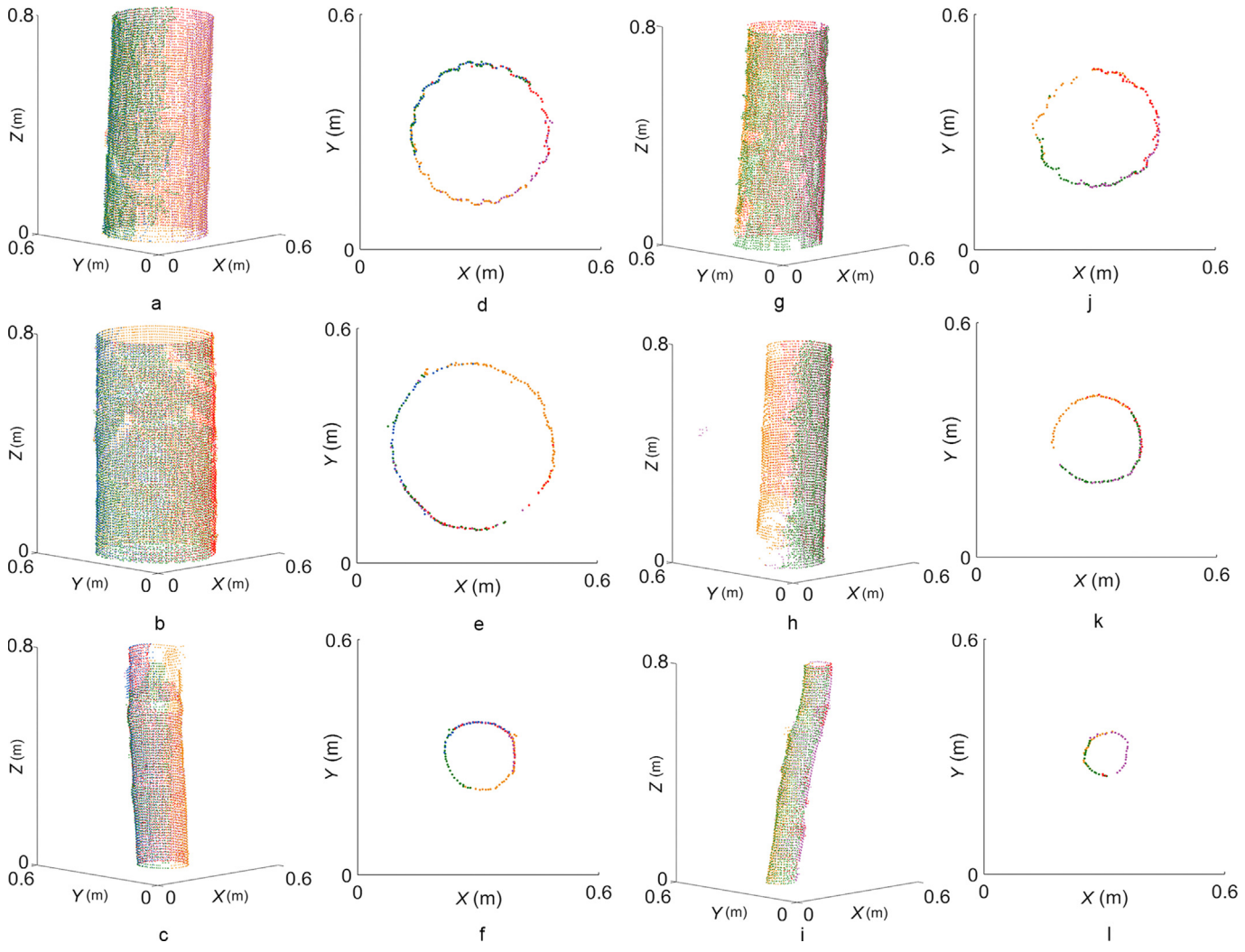

Fig. 9. Examples of the merged tree stem points in three stand complexity categories in the 2D *XY* plane and in 3D for a total of six trees, i.e., two per complex category. From up to down, the rows represent two individual trees from easy, medium and difficult plots, respectively. Points from different scans are illustrated in different colors in each figure. (a–c) and (g–i) show an 80-cm high 3D section around the breast height for each tree. (d–f) and (j–l) show a 1-cm thick cross section of the tree stem around the breast height for each tree. (For interpretation of the references to color in this figure legend, the reader is referred to the Web version of this article.)

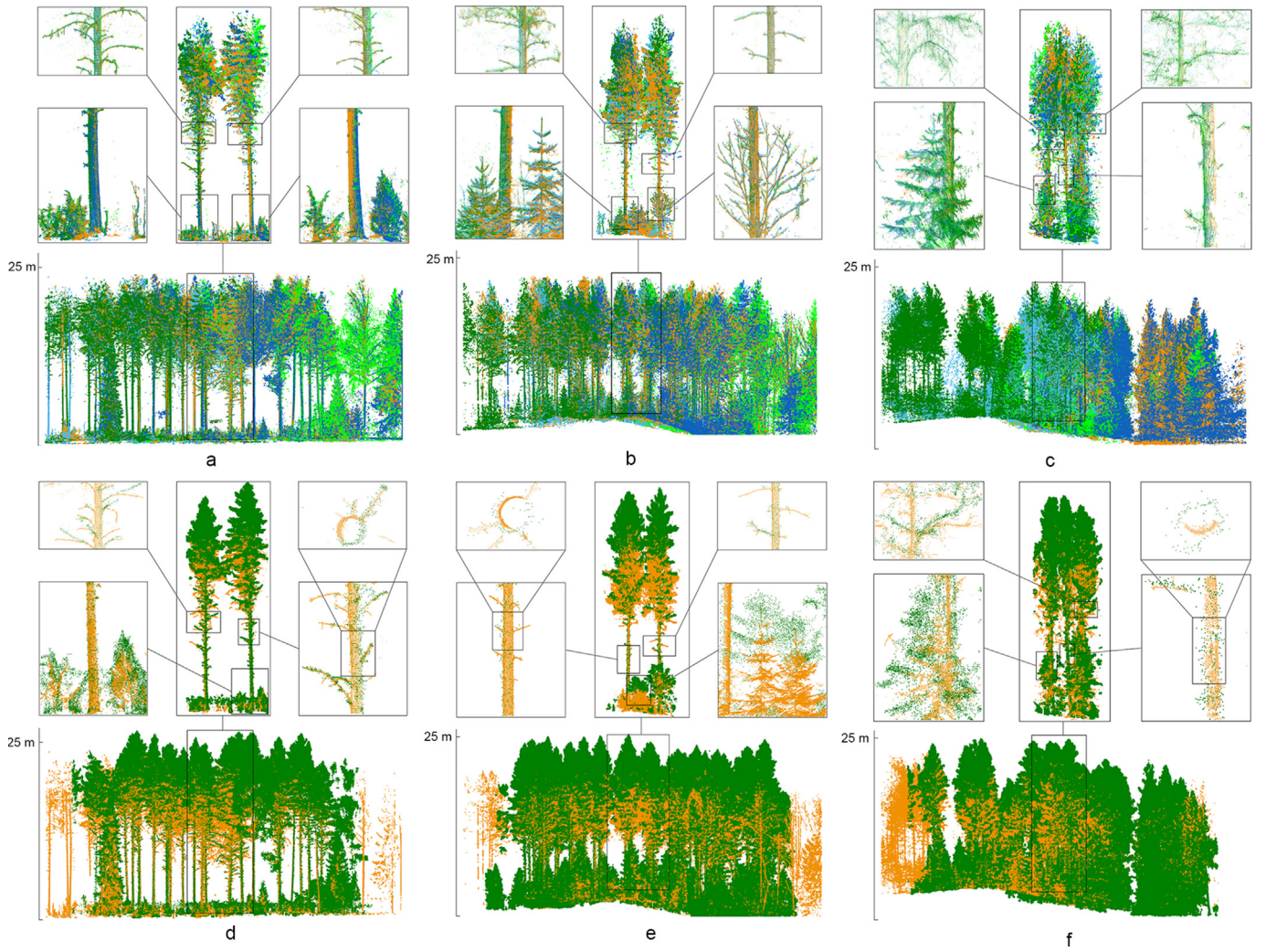

Fig. 10. An illustration of the UAV-TLS registration results in three difficulty categories. Each row with two figures corresponds to one example plot from one of the complexity categories: (a) and (d) to an easy, (b) and (e) to a medium, and (c) and (f) to a difficult plot. (a)–(c) show the TLS point clouds, which were matched pair-wise to the UAV point cloud, i.e., not to each other, as a merged point cloud. (d)–(f) show one of the five TLS point clouds and the UAV point cloud as a merged point cloud. Each color in the figures corresponds to one of the scans and in (d)–(f) the UAV point cloud is depicted in green. (For interpretation of the references to color in this figure legend, the reader is referred to the Web version of this article.)

parameter sets were calculated. The difference in the target-wise errors for an individual point cloud is given by

$$Difference = \sqrt{\frac{1}{N}\sum_{i=1}^{N}\|c_i^R - f_M(c_i^T)\|^2} - \sqrt{\frac{1}{N}\sum_{i=1}^{N}\|c_i^R - f(c_i^T)\|^2} \quad (9)$$

which was applied to evaluate the impacts of the parameter variations between 1) the new registration results obtained by the transformation f_M according to the modified parameters and 2) the reported results obtained by the transformation f using reported parameters.

4.7.3. Generality and applicability of the proposed method

The applicability of the registration method was demonstrated by the registration of static terrestrial and aerial UAV point clouds which corresponds to registering data from different sensors, platforms, and points of time with scene changes. The corresponding data were collected using Leica on the ground and Riegl laser sensors in the air in 2014 and 2017, respectively. Namely, the TLS data was aligned pair-wise with an above-canopy UAV point cloud.

The quantitative accuracy evaluation was carried out using GNSS-based reference data. The center scan locations in each plot were measured in the field in the GNSS coordinate system. The artificial reference targets were then used to derive the positions of the respective border scans. The registration performance was evaluated by the difference between the reference and algorithm-derived scanner positions.

It is worth noting that the reference scanning positions contains GNSS related positing errors, which are in the scale of tens of centimeters under forest canopy (Kaartinen et al., 2015). Thus, the registration error estimates are determined jointly by the algorithm performance and GNSS-measurement accuracy. In addition, the rotation errors are not reflected in the scanner position errors. In short, the positioning accuracy evaluation provides a rough estimation of the accuracy. For these reasons, an example plot in each difficulty category is visually inspected in Section 5.1 for a closer examination.

5. Results

The registration results are reported in three groups, i.e., visual inspection (5.1), quantitative evaluation of the terrestrial registration including both accumulative (5.2) and global registration (5.3), and the evaluation of the registration between different sensors, platforms, and points of time (5.4).

5.1. Visual illustration of the registration results

5.1.1. Registration results between terrestrial observations

Examples of merged terrestrial point clouds at plot and tree levels are illustrated in Fig. 8 in easy, medium, and difficult plots, respectively. Particularly, the merged point cloud in Fig. 8b encompasses the scan with the highest error bound over all scans in the TLS test. As shown in the figures, the registration accuracy is sufficient to capture the details of the branches and stems.

Examples of the tree-stem points in the matched point clouds in easy, medium, and difficult stand complexity categories are illustrated in the 2D *XY* plane and in 3D in Fig. 9. As illustrated, the structure and shape of tree stems are accurately preserved in the merged point cloud.

5.1.2. Registration results between UAV and terrestrial observations

Examples of the merged UAV-TLS point clouds at plot and tree levels are illustrated in Fig. 10 in easy, medium, and difficult plots, respectively. Fig. 10a–c illustrate the terrestrial point clouds based on combining the results from pairwise UAV-TLS registrations. Each color corresponds to one of the scans. These TLS scans are not from a co-registration between TLS point clouds as in Fig. 8, but results of the UAV-TLS registration plotted in the same figure, illustrating the consistency of the UAV-TLS registration results.

Fig. 10d–f illustrate one of the five TLS point clouds and the UAV point cloud as a merged point cloud. The UAV point cloud is depicted in dark green and TLS in yellow in Fig. 10d–f.

The merged TLS point cloud in the easy plot shows the best results with only minor visible differences compared to the TLS registration. Namely, branches and stems are very accurately represented in the merged point cloud, which indicates that the registration between UAV and TLS point clouds was accurate. The merged point cloud in the medium plot is also relatively accurate, although it is visibly less accurate than the merged point cloud from the TLS co-registration. The merged point cloud in the difficult plot is the least accurate of the three. Most of the point clouds are aligned with each other, whereas the close-up on the top left of the merged TLS point cloud shows that the point cloud in green is less accurately aligned with the others. Wind may introduce misalignment in this case, since the registration seems to have a higher accuracy at a lower altitude.

5.2. The accuracy evaluation of the terrestrial registration

The evaluation results according to three quantitative criteria are detailed in 5.2.1–5.2.4. The robustness evaluation is summarized in 5.2.4, and all results are summarized in Appendix. The results are given at both the plot- and scan-level, i.e., as the mean and range of plot-wise average errors and scan-wise errors. Since each plot has an equivalent number of border point clouds, the plot-wise and scan-wise mean errors are always equal, but the error ranges are not. Therefore, the mean errors are reported only at the plot level whereas the same value also represents the scan-wise mean.

5.2.1. Target-wise transformation errors

The target-wise 3D registration errors are presented in Fig. 11. Fig. 11a illustrates the results of the initial registration where most of the errors were in the *Z* direction. Fig. 11b illustrates the final registration results. The mean target error at the plot level was 0.48 cm ranging from 0.31 to 0.91 cm, and the scan-level range was from 0.18 to 1.53 cm. In

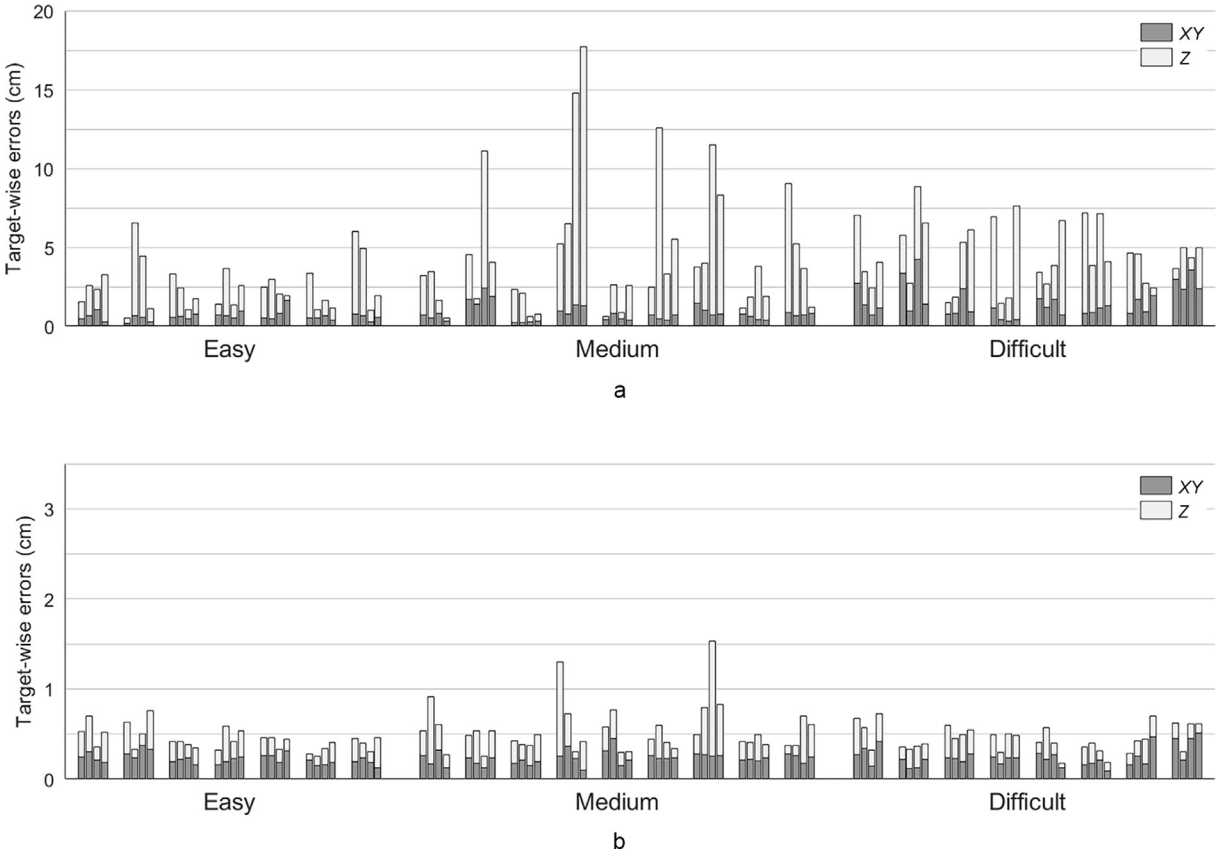

Fig. 11. Target-wise registration errors for each target point cloud in 24 plots of three complexity categories. The four target point clouds within a plot are in the order of accumulative matching from left to right. Each bar represents a target-reference pair, and each plot has 4 bars. The total height of a bar presents the *RMSE* in *XYZ* space from the common target positions between the reference and target point clouds applying the automatically derived registration parameters. In each bar, the bottom (gray) and top (white) parts represent the ratios r_{XY} and r_Z of the errors in *XY* and *Z* directions to the total amount of errors, respectively. (a) The accuracy of the initial registration. (b) The accuracy of the final registration.

general, the target-wise reference registration errors are at the 0.50 cm level. Only seven point clouds have target-wise errors larger than 0.75 cm, which account for approximately 7% of the total amount of the 96 target point clouds.

The easy plots have the smallest registration errors, whereas the results in medium and difficult categories are mostly very similar according to the scan-wise Q_3 statistics in Tables 1 and 3 in the Appendix. The transformation errors in the *XY* and *Z* dimensions were mostly approximately at the same level. The mean target-wise *XY* and *Z* errors were 0.32 cm and 0.34 cm at the plot level. The two cases where the total *XYZ* errors were larger than 1.00 cm have a larger *Z* error component.

It is worth noting that the target-wise reference registration errors have two sources, i.e., the measurement or the point cloud data itself and the registration algorithm. When the reference registration parameters, derived from artificial targets, were applied, the mean target errors were both 0.19 cm, as shown in Fig. 3. Namely, the results presented above also include the uncertainty from the original laser measurements.

5.2.2. Rotation angles and translation differences

The parameter-wise transformation errors are presented for the rotation angles in Fig. 12 and for the translation in Fig. 13. The difference was calculated between algorithm-derived and reference registration parameters.

The total height of a bar in Fig. 12 represents the sum of errors in angles *yaw*, *pitch*, *roll*, and the black, gray, and white parts in each bar correspond to the absolute differences in each angle. The mean errors were 0.11, 0.42, 0.36 mrad at the plot level. Easy forest conditions have the smallest errors, and the registration algorithm has the best and the most stable performance. The results in the medium and difficult categories are similar to each other.

The gray and white parts in each bar in Fig. 13 correspond to the absolute translation differences in *XY* and *Z*, respectively. The total height of a bar represents the sum of the *XY* and *Z* differences. The mean *XYZ*, *XY* and *Z* translation errors were 0.45, 0.26, 0.33 cm at the plot level. The differences between the easy, medium and difficult complexity categories were minor.

5.2.3. The pointwise upper bound errors

The pointwise upper bound estimates the maximum point-wise difference between reference and obtained registration parameters within a distance from the target scanning position. Fig. 14 illustrates the upper bound errors. The total height of a bar represents the upper bound within 10-m distance and the gray part of the bar represents the upper bound within 5-m distance from the observation point. The mean upper bound error was 0.77 cm within 5-m and 1.08 cm within 10-m distance at the plot level.

5.2.4. The robustness evaluation

The robustness of the method concerning the variation of parameter values was evaluated by comparing the TLS registration results derived using different input parameters. As shown in Fig. 15, in the easy stand conditions, the accuracy of the registration results is mostly very stable regardless of the change in parameter values. In medium and difficult stand conditions, most plots showed minor differences, while a few plots

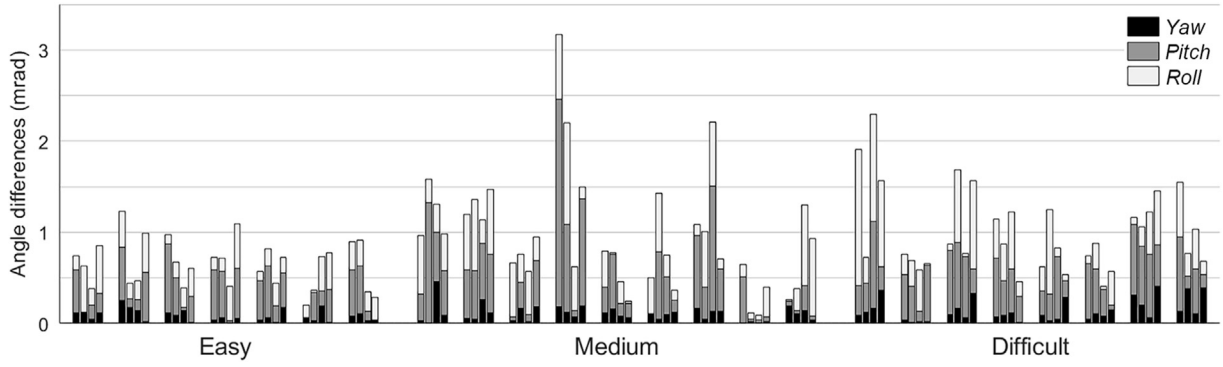

Fig. 12. The differences in registration rotation angles *yaw*, *pitch*, *roll* in 24 plots of three complexity categories. The order of point clouds corresponds to the registration order. Each bar represents a target-reference pair, and each plot has 4 bars. The difference is calculated between the reference and obtained rotation angles. The total height of a bar represents the sum of the differences. The black, gray, and white parts in each bar correspond to the absolute angle differences in *yaw*, *pitch* , *roll*, respectively.

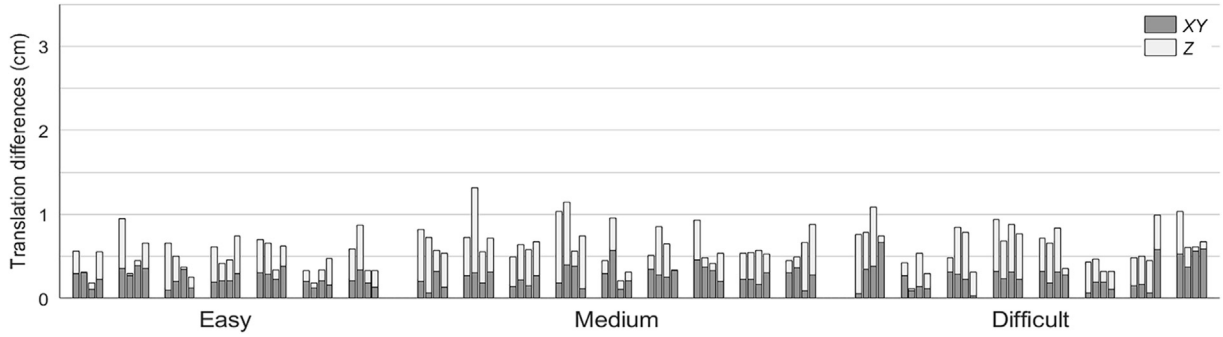

Fig. 13. The difference in the translation in *XY* and *Z* spaces in 24 plots of three complexity categories. The order of point clouds corresponds to the registration order. The difference is calculated between the reference and the obtained translation parameters. Each bar represents a target-reference pair, and each plot has 4 bars. The total height of a bar represents the sum of the differences. The gray and white parts in each bar correspond to the absolute translation differences in *XY* and *Z*, respectively.

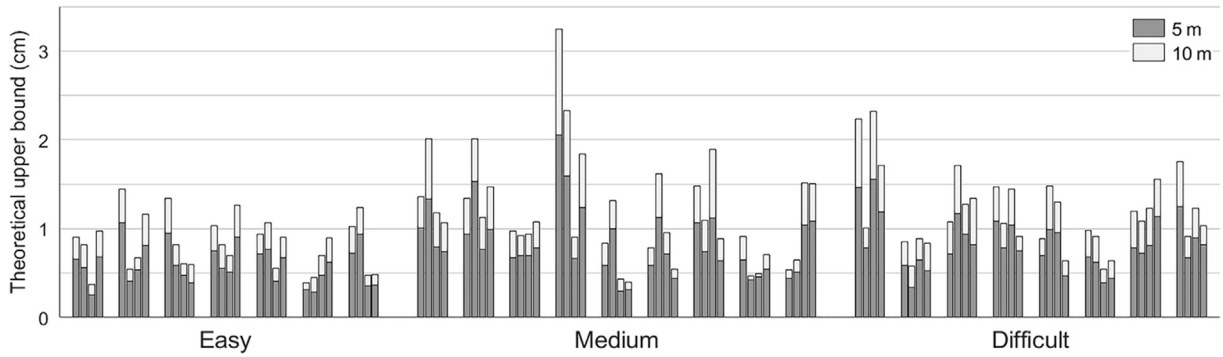

Fig. 14. The theoretical upper bound for the pointwise difference between reference and obtained parameters in 24 plots of three complexity categories. The order of point clouds corresponds to the registration order. Each bar represents a target-reference pair, and each plot has 4 bars. The total height of a bar represents the upper bound at 10-m distance and the gray part of the bar represents the upper bound at 5-m distance from the observation point in the target point clouds.

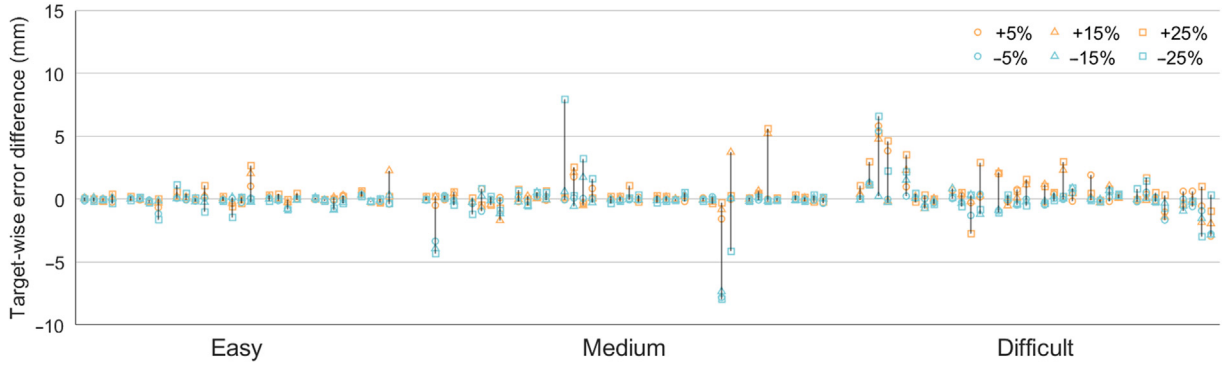

Fig. 15. The parameter sensitivity of the proposed method according to the parameter variation of ±5%, ±15% and ±25%. Each result shows the signed difference in the target-wise errors for individual scans between the reported results and results obtained with modified parameters. The results are grouped according to plots, and each plot contains four target-reference registrations. The order of the results in each plot corresponds to the accumulative registration order in the reported results from left to right.

showed a difference greater than 0.50 cm.

5.3. *The accuracy evaluation of the terrestrial registration with global registration*

Similar to Section 5.2., the results of the TLS registration algorithm supplemented with the global registration step are given as 1) target-wise transformation errors, 2) parameters-wise errors, 3) point-wise upper bound errors, 4) robustness evaluation, which are detailed in 5.3.1–5.3.4 and summarized in the Appendix.

5.3.1. *Target-wise transformation errors*

The target-wise 3D registration errors are presented in Fig. 16. Fig. 16a illustrates the results of the registration with the global registration, and Fig. 16b illustrates the difference to the corresponding results without the global registration step. The mean target error at the plot level was 0.47 cm ranging from 0.26 to 1.03 cm, and the scan-level range was from 0.19 to 1.55 cm. In easy and medium plots, the results with the global registration are in general slightly better than without the global registration, i.e., at the 0.20–0.50-cm level, whereas in the difficult plots the trend is not as apparent. Only ten point clouds have target-wise errors larger than 0.75 cm, which account for approximately 10% of the total amount of the 96 target point clouds. These results showed that the global registration slightly improves the registration accuracy in most cases.

The two plots with excessive increases in errors compared to the registration without the global registration step are discussed in Section 6.

5.3.2. *Rotation angles and translation differences*

The parameter-wise transformation errors are presented for the rotation angles in Fig. 17 and for the translation in Fig. 18.

The mean errors were 0.12, 0.36, and 0.30 mrad at the plot level. Again, the errors were the smallest in the easy forest conditions, where the registration algorithm has the best and the most stable performance. Also, the results in the medium and difficult categories are rather similar to each other. In comparison to the results without global registration, the pitch and roll errors decreased by 0.02–0.10 mrad on average in different difficulty categories, whereas the trend for the yaw angles was less apparent, i.e., both increases and decreases occurred.

The mean *XYZ*, *XY* and *Z* translation errors were 0.41, 0.25, 0.27 cm at the plot level. The differences between the easy, medium and difficult complexity categories were minor. In comparison to the results without the global registration, *Z* translation errors decreased by 0.03–0.08 cm on average in different difficulty categories, whereas the trend in *XY* and *XYZ* translations is less apparent.

5.3.3. *The pointwise upper bound errors*

Fig. 19 illustrates the upper bound errors. The mean upper bound error was 0.69 cm within 5-m and 0.96 cm within 10-m distance at the plot level. The 5- and 10-m upper bound errors decreased on average by 0.12–0.23 cm in easy and medium plots and stayed approximately the same in the difficult plots.

5.3.4. *The robustness evaluation*

Fig. 20 illustrates the robustness of the method concerning the variation of parameter values. The results are similar to those achieved without the global registration. In easy forest conditions, the accuracy of

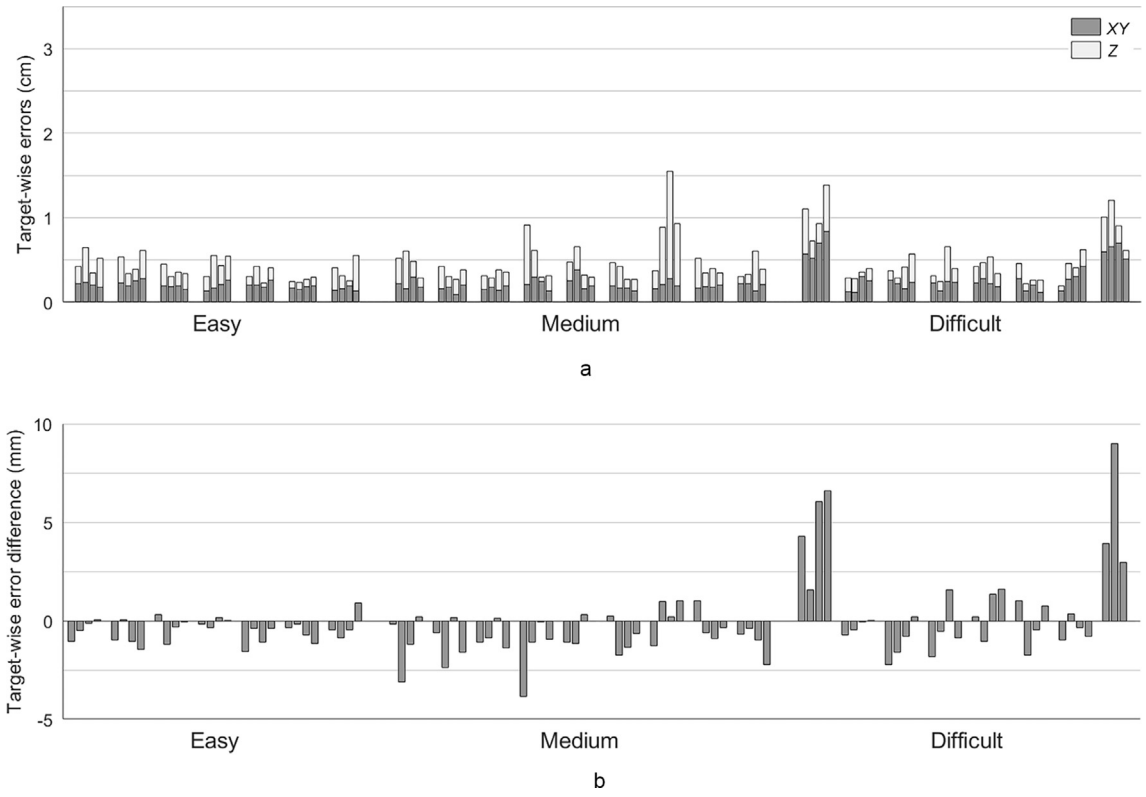

Fig. 16. (a) Target-wise registration errors for each target point cloud in 24 plots of three complexity categories with the global registration step applied, and (b) the differences in results between applying and not applying the global registration in the method. The four target point clouds within a plot are in the order of accumulative matching. Each bar represents a target-reference pair, and each plot has 4 bars. In (a) and (b), the total height of a bar presents the *RMSE* in *XYZ* space from the common target positions between the reference and target point clouds applying the automatically derived registration parameters. (a) In each bar, the bottom (gray) and top (white) parts represent the ratios r_{XY} and r_Z of the errors in *XY* and *Z* directions to the total amount of errors, respectively.

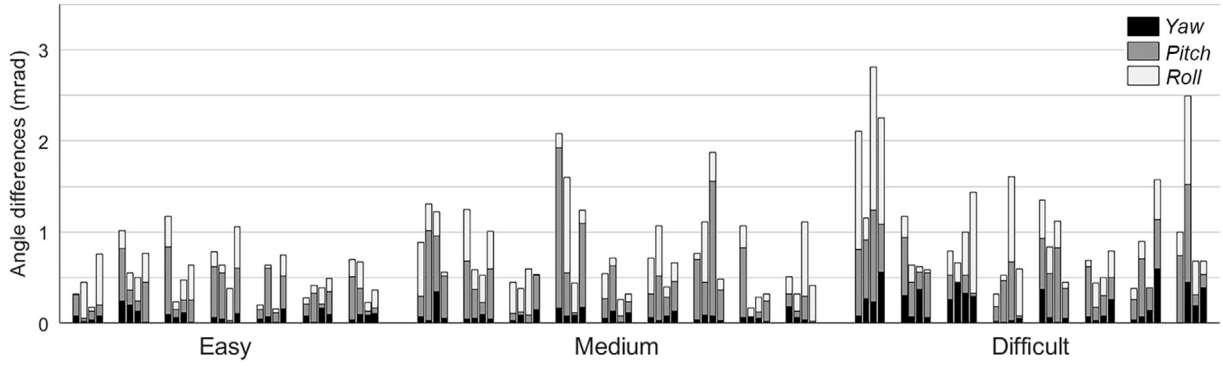

Fig. 17. The differences in registration rotation angles *yaw*, *pitch*, *roll* in 24 plots of three complexity categories. The order of point clouds corresponds to the registration order. Each bar represents a target-reference pair, and each plot has 4 bars. The difference is calculated between the reference and obtained rotation angles. The total height of a bar represents the sum of the differences. The black, gray, and white parts in each bar correspond to the absolute angle differences in *yaw*, *pitch* , *roll*, respectively.

the registration results is mostly very stable regardless of the change in parameter values. In medium and difficult stand conditions, most plots showed minor differences and only one plot showed a difference clearly greater than 0.50 cm. This particular plot exhibited instability also when the global registration was not applied, but in a smaller scale.

5.4. The accuracy evaluation of the registration between different sensors, platforms, and points of time

Fig. 21 illustrates the positional differences between the GNSS-based reference and algorithm-derived scanner positions. On the plot level, the average position differences in easy, medium and difficult plots are 7.2, 12.1 and 13.6 cm, respectively, which are within the level of accuracy of the reference data.

In total, 101 of 110 registrations between terrestrial and aerial observation pairs were successful, i.e., 91.8%. Three scans in medium plots and six scans in difficult plots, depicted in Fig. 21 by the negative-valued bars, did not meet the matching criterion that the distance difference was less than 1m. Discussion on these cases is in Section 6.3.2.

Table 5 represents the statistics of the scan- and plot-wise positioning

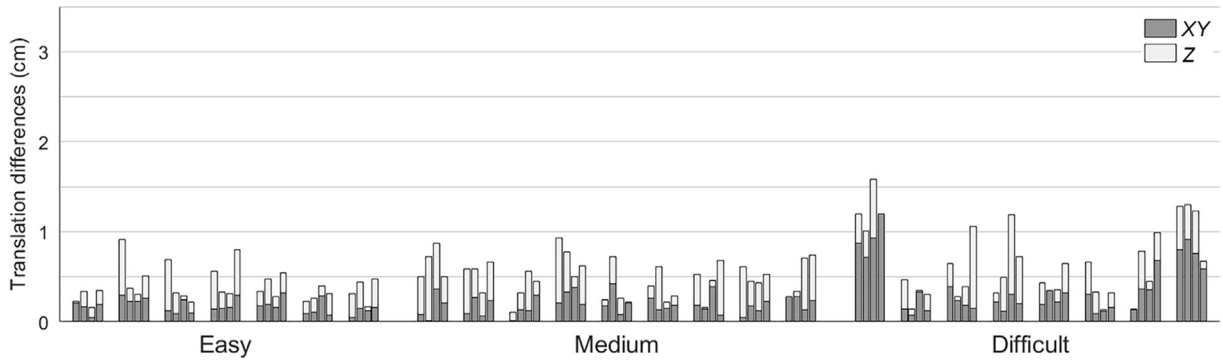

Fig. 18. The difference in the translation in *XY* and *Z* spaces in 24 plots of three complexity categories. The order of point clouds corresponds to the registration order. The difference is calculated between the reference and the obtained translation parameters. Each bar represents a target-reference pair, and each plot has 4 bars. The total height of a bar represents the sum of the differences. The gray and white parts in each bar correspond to the absolute translation differences in *XY* and *Z*, respectively.

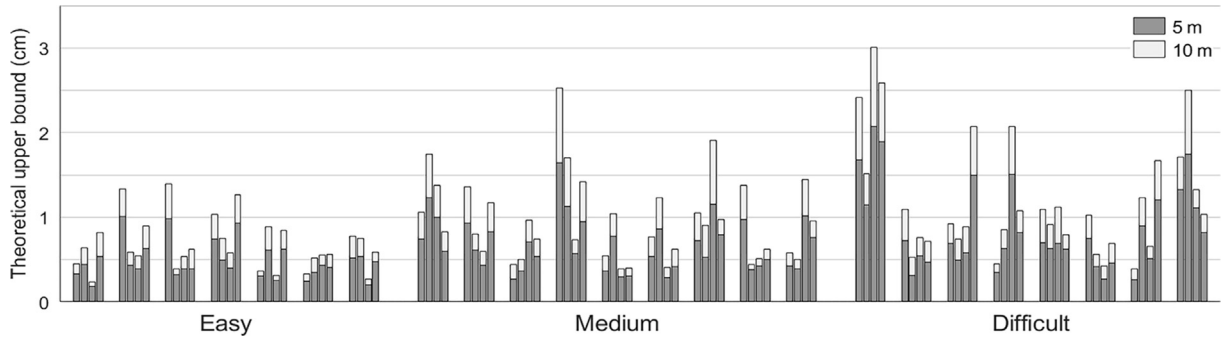

Fig. 19. The theoretical upper bound for the pointwise difference between reference and obtained parameters in 24 plots of three complexity categories. The order of point clouds corresponds to the registration order. Each bar represents a target-reference pair, and each plot has 4 bars. The total height of a bar presents the upper bound at 10-m distance and the gray part of the bar presents the upper bound at 5-m distance from the observation point in the target point clouds.

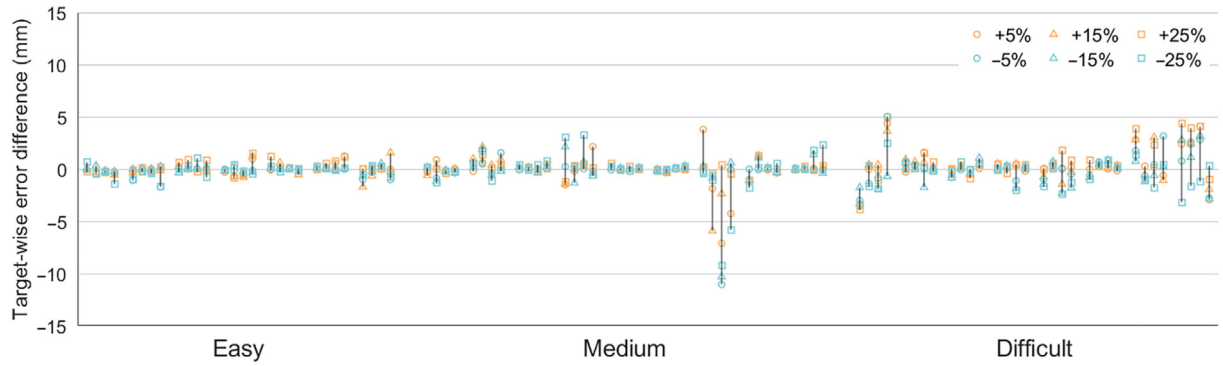

Fig. 20. The parameter sensitivity of the proposed method according to the parameter variation of ±5%, ±15% and ±25%. Each result shows the signed difference in the target-wise errors for individual scans between the reported results and results obtained with modified parameters. The results are grouped according to plots, and each plot contains four target-reference registrations. The order of the results in each plot corresponds to the accumulative registration order in the reported results from left to right.

results.

6. Discussion

This study proposed an automated registration algorithm to retrieve 6 DoF spatial transformation parameters to align wide-baseline point clouds in forests. The experiment and evaluation in this study are the most comprehensive and strict among all previously reported studies. The proposed method was tested using point clouds from both single and multiple sensors, platforms, points of time with scene changes, and different viewpoints, i.e., the terrestrial and aerial viewpoints. The method represents the so far most accurate and robust registration performance, to the best of the authors' knowledge, i.e., sub-cm level errors and the stable performance across different forest difficulty categories and varying parameter values.

In addition, this study proposes a deterministic 2D registration method, which is more stable and robust than sampling methods. Meanwhile, the proposed method represents a new type of mobile mapping, i.e., the stop-and-go mode, which simultaneously solves the problems associated with static and continuous mobile mapping, and opens a door to many other applications.

This section discusses the performance of the registration algorithm

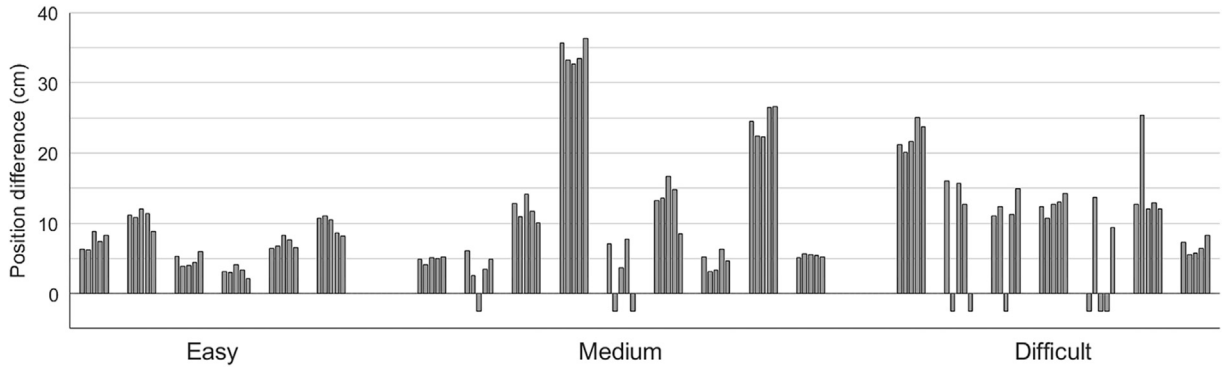

Fig. 21. The difference between reference and algorithm-derived scanner locations for each scan in 24 plots of three complexity categories. Each bar in each plot represents one of the scans in a plot. The height of the bar represents the difference between the reference and the algorithm-derived scanner locations. A negative bar height represents a difference greater than 1 m.

Table 5
Statistics of scan-wise and plot-wise positioning results. The results are reported over all the plots, as well as over easy, medium and difficult complexity categories. Accuracy of the georeferencing results is reported by the minimum, 1st (Q_1), 2nd (Q_2), and 3rd (Q_3) quartiles, maximum and mean of the position error. The erroneously located scans are excluded from the statistics.

	Scan-level position errors (cm)				Plot-level position errors (cm)			
	All	Easy	Medium	Difficult	All	Easy	Medium	Difficult
Min	2.08	2.08	2.58	5.49	3.13	3.13	4.24	6.63
Q_1	5.48	4.44	5.05	10.97	5.38	4.70	4.76	11.78
Q_2	8.82	7.07	7.43	12.68	10.33	7.27	6.17	12.61
Q_3	13.29	8.82	16.63	15.78	13.34	9.82	16.12	14.95
Max	36.28	12.01	36.28	25.44	34.25	10.84	34.25	22.35
Mean	11.33	7.17	12.60	13.80	11.25	7.17	12.13	13.62

from the result, evaluation, and methodology points of view. Practical concerns, and an outlook for future study and applications are also discussed.

6.1. The proposed registration algorithm

According to the experiments, the proposed registration algorithm achieves accurate and robust results for data registration in forests given multi-temporal, sensor, platform point clouds.

To answer the three fundamental questions in the point-cloud registration (see Section 1), the proposed method derives data and feature points as potential correspondences, reconstructs rough observation geometries without external knowledge through the feature-level registration, and retrieves registration parameters at approximately data-level accuracy.

Among the three fundamental questions, selecting stable and representative features and data takes the central position. Registration typically relies on large overlaps to derive correspondences and transformation parameters, e.g., in the dense stereo image matching and in Simultaneous Localization And Mapping (SLAM). These can be assisted by external knowledge through navigation signals such as GNSS and inertial measurement unit. On the contrary, the limited overlap in the sparse sensing or the lack of external knowledge pose significant challenges for the registration. Scenario-related challenges from complicated environments, such as forests, and in situ conditions, such as wind effects, pose additional challenges.

In this study, stable targets and objects that are independent of viewing geometries and invariant throughout the data-acquisition process were chosen to find valid correspondences. The stem-center locations and DTMs were used in the registration as they are robust concerning both varying geometries among observations and incomplete and fragmented objects. For instance, the DTM of a sample plot is relatively robust regardless of the viewpoint. In addition, stem locations and DTM are complementary in the registration since they provide constraints in the *XY* and *Z* directions, respectively.

To answer the second question, i.e., how to establish correspondences between data sets, this study proposed a new 2D point-set registration method. Given deficient overlaps between wide-baseline observations and the lack of external supporting knowledge, to recover observation geometries is particularly important in the registration. The feature-driven strategy has the potential to solve this problem as common features may still be reliably estimated between datasets with even close to zero overlap, e.g., the positions of trees that are standing in-between scanners and are scanned from the opposite directions. More discussion on the 2D registration algorithm is in Section 6.2.

Thirdly, this study proposed DOS and the accumulative mechanism to achieve an accurate and robust registration in the presence of large amounts of structured outliers and in varying conditions. The proposed DOS method finds correspondences in both 2D and 3D registration and in both feature and point cloud space. This approach is applicable to other scenarios and dimensions as long as the matrices, or tensors, can be defined using a suitable coordinate system. DOS finds corresponding data in datasets with limited overlaps, and thus enables the data-driven method to improve the final registration accuracy by taking advantage of the highly accurate laser measurement and by avoiding deriving locally optimal solutions.

The accumulative mechanism in the proposed method allows the reference data set to grow as new data sets are matched and integrated. Accordingly, the probability of a successful registration increases, since the larger overlap area increases the number of common features and the potential for a successful matching. The downside of the accumulation is that it relies on the correctness of previous matches, which emphasizes the importance of robustness in each step of the registration algorithm. The optional global registration step utilizing the Lie-algebraic motion averaging algorithm was introduced as a potential cure to the possible error accumulation. Due to the wide-baseline setup and low overlaps,

Table 6
The parameter-level registration errors reported in the previous research and in this work. The results are presented as the plot-wise average errors, the range of plot-wise average errors, and the range of scan-wise errors. Unreported results in the original literature are denoted by a dash-line. The results in the previous research were reported using the same number of digits as in the original papers.

Research	Plots	Translation errors (cm)					Angular errors (mrad)		
		t_{xyz}	t_{xy}	t_x	t_y	t_z	φ	θ	ψ
Ni et al. (2011)	1	–	–	2.1	1.8	7.6	–	–	–
		–	–	–	–	–	–	–	–
		–	–	0.3–4.5	1.1–2.4	1.5–22.0	–	–	–
Kelbe et al. (2016)	11	–	–	7.8	7.2	12.4	3.3	8.4	16.3
		–	–	–	–	–	–	–	–
		–	–	–	–	–	–	–	–
Liu et al. (2017)	10	–	1.08	–	–	6.29	0.88	–	–
		–	0.39–2.88	–	–	1.26–18.26	0.28–2.51	–	–
		–	0.10–6.44	–	–	0.14–71.81	0.04–4.78	–	–
Tremblay and Béland (2018)	5	8.3	–	1.4	1.3	7.7	1.3	4.3	9.4
		1.6–13.7	–	0.3–3.1	0.1–2.5	1.6–13.6	0–3.3	0.5–9.1	1.2–16.1
		0.7–40.4	–	0.2–14.6	0–6.4	0–37.6	0–10.8	0–13.2	0.7–46.3
Dai et al. (2020)	10	7.45	1.13	–	–	7.21	0.61	–	–
		2.03–20.27	0.58–2.00	–	–	1.67–20.11	0.16–1.26	–	–
		–	–	–	–	–	–	–	–
This work (without global reg.)	24	0.45	0.26	0.18	0.16	0.33	0.11	0.42	0.36
		0.24–0.69	0.14–0.51	0.08–0.32	0.05–0.34	0.16–0.60	0.01–0.25	0.10–1.12	0.15–0.97
		0.09–1.06	0.03–0.66	0.01–0.56	0–0.57	0.01–1.02	0–0.46	0.01–2.27	0.02–1.49
This work (with global reg.)	24	0.41	0.25	0.18	0.14	0.27	0.12	0.36	0.30
		0.21–1.01	0.12–0.93	0.07–0.81	0.04–0.36	0.11–0.48	0.03–0.33	0.12–0.80	0.09–1.07
		0.09–1.19	0.01–1.19	0–1.07	0–0.57	0–0.91	0–0.59	0–1.76	0–1.57

only those global registration methods that don't require the applied key points to have correspondences in each point cloud, e.g., the presented method, are applicable.

All these measures supported a robust solution to answer the three fundamental questions. According to the experiments, the registration results among the three forest complexity categories are stable despite the significant challenges posed by more complicated forest stand conditions. The stability and the achieved results indicated that these measures are effective in identifying effective features and correspondences under heavy disturbances in forest environments.

The approach presented in this paper is expected to be scalable to larger data sets with more than a few point clouds. The wide-baseline approach and the overlap search make sure that the number of points applied in the ICP step stays reasonable for the final registration step. In any case, if shorter baselines were applied, resulting in a larger number of point clouds per plot, point sampling can always be applied to decrease the hardware requirements. As for the 2D matching algorithm, the complexity is proportional to the number of points, i.e., stems, in the registration, which is related to the study area and its stem density rather than the number of scans. Sampling strategies can be applied to the 2D algorithm as well in order to speed up the process. Testing the scalability of the method in detail would, however, require tests with multiple point clouds, which is outside the scope of this study.

6.2. The 2D point sets registration

This study proposed a new 2D point sets registration method to roughly reconstruct the observation geometry. In noisy wide-baseline point clouds, arbitrary matches, i.e., point pairs without any meaningful correspondences, may show stronger matching patterns than the true matching pairs. Thus, the 2D point sets registration has to take the high noise level into consideration.

The performance of the proposed 2D matching method is comparable with RANSAC. In a test of matching four border scans to their corresponding center scans in 24 plots, i.e., a total of 96 pairwise matches, the proposed algorithm failed to match 3 scans from 2 difficult plots in total. RANSAC mostly got the same results. It failed in the same three scans as the proposed 2D matching method, and failed in another one or two scans depending on the parameter settings. That is, RANSAC failed in four or five scans with probability parameter $p = 0.9$, and failed in four scans with $p = 0.99$.

The advantage of the proposed 2D matching method lies in that it is a deterministic method that gives the same results in each implementation, which can be a preferable characteristic in applications where the emphasis is on the stability. On the contrary, sampling-based methods such as RANSAC may or may not work depending on the sampling results.

Another deterministic registration method, i.e. Coherent Point Drift (CPD) (Myronenko and Xubo Song, 2010), was also tested in the pairwise

Table 7
The target-level registration errors using artificial reference targets reported in the previous research and in this work. The results are presented as the plot-wise average errors, the range of plot-wise average errors, and the range of scan-wise errors (The results in Zhang et al. (2021) are incomparable and excluded from this table since they were not evaluated using artificial reference targets.).

Research	Plots	Target-level errors (cm)		
		T_{xyz}	T_{xy}	T_z
Guan et al. (2020)	6	4.2	–	–
		2.4–6.8	–	–
		–	–	–
This work (without global reg.)	24	0.48	0.32	0.34
		0.31–0.91	0.22–0.51	0.17–0.81
		0.18–1.53	0.12–0.63	0.07–1.50
This work (with global reg.)	24	0.47	0.32	0.31
		0.26–1.03	0.20–0.88	0.12–0.89
		0.19–1.55	0.12–1.16	0.06–1.52

matching with an exhaustive test over the space of possible parameter settings. With the best parameters found, CPD was able to find the correct registration for four of the 96 scans, i.e., 4.2%. Likely contributors to such a result include an unfavorable initial alignment of the point clouds, noise, and a high number of outliers. Indeed, using the best CPD parameters found, when an arbitrary initial rotation was applied to the target point clouds, the registration failed for all four previously successful scan pairs while succeeding for five different scan pairs. This emphasizes the advantage of methods that are independent of initial alignment.

6.3. The results

6.3.1. TLS registration

Table 6 summarizes the parameter-level registration errors reported in the previous research, and the corresponding errors in this work, i.e., the translation errors in 3D (horizontal, X, Y, and Z spaces denoted by t_{xyz}, t_{xy}, t_x, t_y and t_z) and the angular errors with respect to Z, Y, and X axes (denoted by φ, θ, and ψ, which in the case of this work correspond to *yaw*, *pitch*, and *roll*, respectively). The results presented in the table comprise the average of plot-wise errors, the range of plot-wise average errors, i.e., minimum and maximum, and the range of scan-wise errors. A dash-line indicates unreported results. Table 7 reports the same statistics over the target-level errors based on the artificial reference targets. In general, the proposed method achieved roughly an order of magnitude smaller registration errors than what has been reported previously.

Among all three rotation parameters, the error in the *Yaw* angle around the Z axis is typically the smallest, i.e., much smaller than the errors in the other two rotation angles. In terms of the translation parameters, the Z translation parameter is more challenging to derive. Similar trends were also reported in Ni et al. (2011), Kelbe et al. (2016), Liu et al. (2017), Tremblay and Béland (2018), Dai et al. (2020). In the Z direction, because of the high similarity of the stems, most of the stem points do not contribute to the registration at the level of accuracy that is needed for a precise registration.

In terms of the absolute registration accuracy, i.e., the difference of artificial target centers between the reference and the target point clouds, the results were at the 0.50-cm level in most of the individual scans across different sample plots. The two cases with scan-level registration errors above 1.0 cm suffered from unreliable corresponding points. The noisiness and concentrated distribution of the extracted points, caused by both the point extraction methods and the forest conditions, e.g., the viewing geometry, slopy terrain and occlusion effects, reduced the registration accuracy, especially in the Z direction.

The maximum achievable accuracy of the registration is mostly determined by the accuracy of the raw point cloud, given that all method-related factors have been excluded. Uncertainties exist in the point clouds, which are mainly determined by the system mechanism and measurement conditions, e.g., calibration, the range measurement accuracy and the beam divergence (Liang et al., 2016). The magnitude of these uncertainties is typically small, e.g., at mm level, as shown in the sphere fitting in Section 3.3. Considering this and the registration results, the achieved accuracy is close to the accuracy of the raw point cloud.

The sensitivity test revealed that the proposed method gave very similar results when the parameters were decreased and increased by up to 25%. Only four point clouds showed target-wise error differences greater than 0.50 cm. The results indicated that moderate changes in the input parameter values of the algorithm have mostly minor impact on the registration results when the amount and spatial distribution of reliable correspondences are sufficient.

Applying the global registration method had in general a slight positive effect on the accuracy in easy and medium plots, whereas in difficult plots the effect is more ambiguous and seems to depend on the scene. In particular, two plots with highly demanding forest conditions, e.g., low visibility and low number of correspondences, exhibited an increase in errors of around 0.50 cm when applying the global registration after the accumulative registration. These two plots showed stable results in the stability analysis when applying the global registration, which indicates that the reason behind the error increases is not in the choice of parameters. Since the global registration was based on pair-wise registration and the two plots were from the difficult category, most likely the low overlap in these two plots caused the pair-wise results to be more erroneous than the accumulative results.

According to the results, the global registration step may not be strictly necessary in the registration since it only improved the results slightly. Meanwhile, it adds both implementational and computational complexity to the method. Hence, omitting the global adjustment a fully viable option.

It is worth emphasizing that the statistics in Tables 6 and 7 were computed over all plots, and since the results in difficult plots were on average worse than in easy and medium plots, inspecting the averages over all plots makes the results with and without the global registration seem rather similar to each other.

Overall, the proposed method is robust concerning the parameter values in most of the investigated forest stand conditions. The complexity of the forest stand has a limited impact on the parameter sensitivity of the method. The differences are in general small in easy and medium conditions, whereas difficult conditions exhibit slightly higher variations.

6.3.2. UAV-TLS registration

The sparsity, lower accuracy, and concentrated distribution of the UAV point clouds are clearly visible in Fig. 10d–f. Namely, the UAV point clouds have a much lower point density than the TLS counterparts because of the larger scan-object distances, and a much higher level of the inconsistency stemming from the errors in the mobile system, which can be seen for example in Fig. 10f where the stem cross-section close-up on the right shows a heavily distorted stem shape. Furthermore, as seen from the plot-views of each figure, most of the UAV data are concentrated on the tree crowns and ground, while coverage on the stems is much sparser than that from the terrestrial point of view.

The low density, inconsistency, and low number of points captured on the stems in the UAV point clouds limit the highest achievable accuracy in the UAV-TLS registration. That is, unlike in the TLS co-registration, it is not realistic to expect millimeter level errors since the data contains centimeter level errors. However, based on visual inspection, centimeter-level errors are feasible in the UAV-TLS registration.

In addition to the lower accuracy expectations in the UAV-TLS registration compared to the TLS co-registration, the method is also more prone to fail due to low overlap and errors in the UAV point clouds. Nine of the 110 pair-wise matches failed since the planar registration was unable to reconstruct the rough geometry. In these nine cases, the UAV and TLS point clouds had only few common trees, i.e., between 4 and 10. The low overlap and inaccurate stem locations in the UAV data can evidently lead to a failure in the planar registration and consequently to the failure of the entire registration. One way to tackle this problem, while outside the scope of this paper, would be to first co-register the TLS point clouds, which increases the overlap between TLS and UAV data, and then perform the registration between the merged TLS and the UAV point clouds.

Overall, the results demonstrate the applicability of the method to multi-temporal, senor, platform datasets and promote research toward georeferencing the under-canopy terrestrial point clouds using above-canopy UAV measurements and automated point cloud registration. More discussion is in Section 6.5.

6.4. The evaluation

The performance of the proposed method was extensively tested in 24 forest sample plots of varying boreal forest conditions, which represents the largest test data set and the most diverse forest conditions for automated registration methods thus far to the best of the authors' knowledge.

The example cases of the different forest stand complexity categories

are illustrated in the Figs. 1, 8 and 10. The easy plots have a good horizontal visibility due to sparsely distributed trees, low number of young trees and Scots pine being the dominant tree species. The medium plots show already much worse visibility due to a denser tree distribution and a significantly higher number of young trees. The difficult plots show very low horizontal visibility due to a denser tree population with more spruces and small trees.

The registration results were evaluated by three evaluation criteria in this study. The three evaluation criteria have their respective pros and cons.

The center points of the artificial 3D reference spheres placed in the field provide the most reliable reference data for the evaluation of the registration results. They do not rely on any additional sensors, e.g., total station, and thus are free from any additional measurement errors. This evaluation gives an absolute measure of matching accuracy, which indicates the average registration accuracy in the study area through individual objects distributed within the plot.

In contrast, the difference between the reference and derived registration parameters is a relative measure with respect to the reference registration parameter. The parameter differences barely give any indication of the error magnitude at spatial positions, e.g., the same angular difference gives much greater errors at a further distance than close to the rotation center.

In addition to the conventional target and parameter evaluation criteria, an error upper bound was used as the third criterion to evaluate the registration accuracy in point clouds. The upper bound of the position errors is a relative evaluation criterion. It compensates for the downsides of the parameter- and object-level error estimates by uniting all parameter-level errors into a single quantity and by indicating the maximum point-wise difference in 3D between the reference and retrieved registration parameters at any position within a given distance from the target scanner location.

The data acquisition related errors are also present in the registration errors, i.e., from the applied TLS equipment and the data acquisition process in this case. According to the results in Fig. 3, the target-wise errors of the reference registration parameters at the scan level were between 0.03 and 0.40 cm and had a mean value of 0.19 cm, which is in the scale of the measurement accuracy given by the scanner, i.e., a few millimeters.

6.5. Further development and practical concerns

The proposed method applied a series of solutions to find correspondences between observations and to filter unreliable candidates. These measures effectively answer the three fundamental questions in the point cloud registration and work well according to the experiment.

It is worth noting that the proposed solution is an open framework. Solutions applied in individual steps in the current proposed algorithm may be replaced by any new solution with improved performance. For example, any 2D matching method that meets the robustness requirement can be used to reconstruct the rough observation geometry. In the further development, the key issue is to select robust methods in the individual steps that can handle the low signal-noise-ratio problems of wide-baseline data. New superior solutions should improve the overall performance of the proposed algorithm.

Given the intrinsic high noise level in the sparse sensing, the registration may fail when the baseline is too large. The exact tolerable distance between observations depends on the forest stand conditions, and partly on the instrument performance, e.g., angular resolution, scanning frequency/speed and distance measurement accuracy. In general, the largest tolerable baseline should be larger in easy forest conditions than that in the complex conditions. For example, a baseline greater than 10 m in a complicated forest may significantly increase the risk of a failure in the registration in boreal forests.

According to the registration results in this study, the quality of the data is the determining factor for a successful registration. Given sufficient data quality, e.g., geometric accuracy, consistency, visibility, and overlaps, a properly designed algorithm is capable of aligning individual observations. On the contrary, given insufficient data quality, the best algorithm cannot, or at least has tremendous difficulties to, give any accurate solution. The dominant role of the data quality in feature extraction was also reported in other previous studies, e.g., Wang et al. (2019b).

It is worth noting that the quality is jointly determined by the hardware, forest conditions, and data-acquisition. Any conclusions drawn without considering these factors are bold. On the other hand, all these factors need to be carefully taken into consideration before the data collection in order to achieve a successful registration.

6.6. Outlook

In addition to being a new registration algorithm for wide-baseline observations, the proposed method provides solutions for numerous new applications, such as 1) the global positioning of individual under-canopy observations, 2) the fusion of point clouds acquired from terrestrial and aerial perspectives, 3) mobile mapping using a new stop-and-go approach, 4) point cloud registration using a short-baseline dense data-acquisition pattern.

The proposed method serves as a solution to locate an individual observation in a known system. One of the biggest problems of the static terrestrial observations is that the data collected are in local coordinate systems whereas their absolute positions are unknown, thus limiting the effectiveness of the field reference data. To put such local observations reliably into a global system is challenging considering that the conventional GNSS positioning solutions are prone to errors and high variances according to satellite and forest conditions.

The UAV-TLS data registration scenario in this study demonstrated the applicability of locating local observations in global systems through UAV observations. In general, the observations here can be from any platform having sufficient data quality. For instance, the terrestrial data can be collected by a harvester, mobile mapping system, or under-canopy UAV (Hyyppä et al., 2020a; Wang et al., 2021), whereas the UAV data represent the reference data with known coordinates that can also be collected using any static, mobile, or aerial platform.

Remote sensing has the potential to capture the tree top and canopy information more comprehensively and efficiently in comparison with conventional terrestrial observations (Wang et al., 2019a; Jurjević et al., 2020). However, the visibility of the tree-top from remote sensing data is not guaranteed in static terrestrial observations (Liang et al., 2018a). The mobile mapping may solve this problem in sparse forests, but may still face challenges in dense canopy conditions (Balenović et al., 2021; Hyyppä et al., 2021; Liang et al., 2022). The fusion of point clouds acquired from terrestrial and aerial perspectives is one of the key solutions for achieving a complete forest observation (Wang et al., 2019a, 2021). As shown in the experiments in the registration of the above-canopy UAV and under-canopy terrestrial observations, the door for automated fusion of terrestrial- and aerial-acquired point clouds has now been opened.

The proposed method also represents a new type of mobile mapping approach, i.e., the stop-and-go mode, where the platform carries sensors in the forest while the data is collected statically at particular locations. Up to now, the continuous approach has been the dominating mobile data-acquisition mode, i.e., the data are collected along with the platform movement. However, soon after starting the data collection, clear distortions are expected due to the platform movement and the scanning mechanism. Thus far, such distortions have either been ignored or roughly compensated using sensor position and orientation, e.g., through linear interpolations. Since it is very challenging to precisely compensate such distortions for each point, the accuracy of the mobile mapping system is inevitably lower than that of the static systems. In comparison with scanning sensors, planar frame sensors such as cameras or flash Lidar have less distortion problems but suffer from the blurred data caused by the platform movement.

The stop-and-go approach not only solves the problems of lacking mobility and slow data collection in static terrestrial measurements, but also solves the data-quality issue in the continuous mobile approach. The challenge faced by the stop-and-go mobile approach is actually the lack of robust registration methods for wide-baseline observations since short-baseline observations are cost-ineffective and impractical.

Thus far, the stop-and-go approach has not been widely adopted or applied. The test data in this study, i.e., multi-scan static data, simulates the stop-and-go mobile approach. Thus, the path to apply the stop-and-go mobile approach has been paved, and further studies should start to explore the potential and benefits of the stop-and-go mobile approach, especially the combination of precise data and high data-collection efficiency.

It is also worth noting that methods which work for wide-baseline observations are also applicable to short-baseline observations, but not necessarily vice versa.

7. Conclusions

The challenges of point cloud registration in forest conditions stem from different perspectives. Complicated forest conditions significantly limit the visibility in the forest and forest point cloud data, and consequently the amount of mutual targets available for registration purposes. The sparse data acquisition introduces significant changes in viewing geometry and further decreases the already limited overlap. This work presented an automated registration algorithm to tackle the problem of matching wide-baseline terrestrial point clouds.

The proposed method derives data and feature points as potential correspondences. The registration reconstructs rough observation geometries without external knowledge on the feature-level and retrieves precise registration parameters on the data level using discrete overlap search (DOS) to find sufficient correspondences. The method works with an accumulative concept such that the reference scan grows step by step while matched target scans are added to the reference scan, which increases the probability of a successful registration along with the growth of the reference scan. The new 2D registration method that works in noisy data sets provides a deterministic solution, which is suitable for applications requiring stable results and is an alternative to the sample-based methods. The work also proposed an error upper bound that quantitatively indicates the largest pointwise registration uncertainty, which compensates for the downsides of the two widely used parameter- and object-level error estimates by uniting all parameter-level errors into a single quantity.

The algorithm was tested in 24 sample plots of varying forest conditions that were classified into three difficulty categories. According to the accumulation registration results, the proposed method achieved a 3D registration accuracy at a 0.50-cm level in all three difficulty categories. The averages over 3D translation errors and the three rotation angles were 0.45 cm and 0.11–0.42 mrad. The average upper bound errors at 5 and 10 m were 0.77 and 1.08 cm, respectively. These results represent the so far most accurate automated registration results with a strict evaluation. The results were slightly improved in easy and medium plots with the global matching, whereas the trend in difficult plots was less apparent and seemed to depend on the particular forest conditions.

The proposed method was tested for stability in the sensitivity test where the method gave very similar results when the parameters were decreased and increased by up to 25%. The results indicated that the proposed method is robust concerning the parameter values in most of the investigated forest stand conditions. Moderate changes in the input parameter values of the algorithm and the complexity of the forest stand had mostly minor impact on the parameter sensitivity of the method and on the registration results.

In addition to the above test using a single terrestrial sensor at a particular point of time, the proposed algorithm was also tested between terrestrial and aerial point clouds, between data captured by multiple hardware, and between data recorded at different points of time with scene changes. According to the visually inspected merged point clouds, the easy and medium plots showed relatively accurate alignment between aerial and terrestrial point clouds, whereas the registration in the difficult plot was less accurate. The average position differences in easy, medium and difficult plots are 7.2, 12.1 and 13.6 cm, respectively, according to the reference target positions, which are within the level of accuracy of the reference data.

These extensive tests indicate that the automated registration method can achieve millimeter-level accuracy in typical boreal forest conditions for wide-baseline point clouds, as long as the point cloud data themselves have sufficient quality, e.g., geometrical accuracy and point density.

Furthermore, the proposed method is applicable in dense sensing which is a less demanding problem. The proposed method also provides solutions to multiple scenarios such as the global positioning of individual under-canopy observations, and the registration between terrestrial and aerial datasets. The method also supports a new mobile mapping approach, the stop-and-go mode, where the measurements are collected statically with wide-baseline observations while sensors are carried by a mobile platform, which solves the problems of lacking mobility and slow data collection in static terrestrial measurements, as well as the data-quality issue in the continuous mobile approach.

Fundings and acknowledgements

The authors would like to acknowledge financial support from the National Natural Science Foundation of China (Grant Nos. 32171789, 32211530031), Wuhan University (No. WHUZZJJ202220), Academy of Finland (Nos. 334060, 334829, 331708, 344755, 337656, 334830, 293389/314312, 334830, 319011).

Author contributions

Xinlian Liang designed the concept of the method. Onni Pohjavirta and Xinlian Liang developed the method and carried out the experiment. Xinlian Liang, Onni Pohjavirta and Yunsheng Wang carried out the analysis of results and prepared the manuscript. Yunsheng Wang, Jiri Pyörälä, Antero Kukko, Eric Hyyppä, Xiaowei Yu, Harri Kaartinen and Juha Hyyppä provided the original data, the references, and other resources required by the experiment. All contributed to the finalization of the manuscript.

Availability of data and materials

The datasets used and/or analyzed during the current study are available from the corresponding author on reasonable request.

Declaration of competing interest

The authors declare that they have no known competing financial interests or personal relationships that could have appeared to influence the work reported in this paper.

Appendix A. Supplementary data

Supplementary data to this article can be found online at https://doi.org/10.1016/j.fecs.2022.100080.

References

Balenović, I., Liang, X., Jurjević, L., Hyyppä, J., Seletković, A., Kukko, A., 2021. Hand-held personal laser scanning: current status and perspectives for forest inventory application. Croat. J. For. Eng. 42, 163–174. https://doi.org/10.5552/crojfe.2021.858.

Bienert, A., Maas, H.-G., 2009. Methods for the automatic geometric registration of terrestrial laser scanner point clouds in forest stands. In: Bretar, F., Pierrot-Deseilligny, M., Vosselman, G. (Eds.), Laser Scanning 2009. ISPRS, Vol. XXXVIII, Part 3/W8, Paris, France, September 1-2, 2009.

Borrmann, D., Elseberg, J., Lingemann, K., Nüchter, A., Hertzberg, J., 2008. Globally consistent 3D mapping with scan matching. Robot. Autonom. Syst. 56, 130–142. https://doi.org/10.1016/j.robot.2007.07.002.

Crum, W.R., Hartkens, T., Hill, D.L.G., 2004. Non-rigid image registration: theory and practice. BJR 77, S140–S153. https://doi.org/10.1259/bjr/25329214.

Dai, W., Yang, B., Liang, X., Dong, Z., Huang, R., Wang, Y., Pyörälä, J., Kukko, A., 2020. Fast registration of forest terrestrial laser scans using key points detected from crowns and stems. Int. J. Digit. Earth 1–19. https://doi.org/10.1080/17538947.2020.1764118.

Durrant-Whyte, H., Bailey, T., 2006. Simultaneous localization and mapping: part I. IEEE Robot. Autom. Mag. 13, 99–110. https://doi.org/10.1109/MRA.2006.1638022.

Govindu, V.M., 2004. Lie-algebraic averaging for globally consistent motion estimation. In: Proceedings of the 2004 IEEE Computer Society Conference on Computer Vision and Pattern Recognition, 2004. CVPR 2004. IEEE, Washington, DC, USA, pp. 684–691. https://doi.org/10.1109/CVPR.2004.1315098.

Guan, H., Su, Y., Hu, T., Wang, R., Ma, Q., Yang, Q., Sun, X., Li, Y., Jin, S., Zhang, J., Ma, Q., Liu, M., Wu, F., Guo, Q., 2020a. A novel framework to automatically fuse multiplatform LiDAR data in forest environments based on tree locations. IEEE Trans. Geosci. Rem. Sens. 58, 2165–2177. https://doi.org/10.1109/TGRS.2019.2953654.

Guan, H., Su, Y., Sun, X., Xu, G., Li, W., Ma, Q., Wu, X., Wu, J., Liu, L., Guo, Q., 2020b. A marker-free method for registering multi-scan terrestrial laser scanning data in forest environments. ISPRS J. Photogrammetry Remote Sens. 166, 82–94. https://doi.org/10.1016/j.isprsjprs.2020.06.002.

Henning, J.G., Radtke, P.J., 2008. Multiview range-image registration for forested scenes using explicitly-matched tie points estimated from natural surfaces. ISPRS J. Photogrammetry Remote Sens. 63, 68–83.

Henning, J.G., Radtke, P.J., 2006. Ground-based laser imaging for assessing three dimensional forest canopy structure. Photogramm. Eng. Rem. Sens. 72, 1349.

Hilker, T., Coops, N.C., Culvenor, D.S., Newnham, G., Wulder, M.A., Bater, C.W., Siggins, A., 2012. A simple technique for co-registration of terrestrial LiDAR observations for forestry applications. Remote Sens. Lett. 3, 239–247. https://doi.org/10.1080/01431161.2011.565815.

Hyyppä, E., Hyyppä, J., Hakala, T., Kukko, A., Wulder, M.A., White, J.C., Pyörälä, J., Yu, X., Wang, Y., Virtanen, J.-P., Pohjavirta, O., Liang, X., Holopainen, M., Kaartinen, H., 2020a. Under-canopy UAV laser scanning for accurate forest field measurements. ISPRS J. Photogrammetry Remote Sens. 164, 41–60. https://doi.org/10.1016/j.isprsjprs.2020.03.021.

Hyyppä, E., Kukko, A., Kaijaluoto, R., White, J.C., Wulder, M.A., Pyörälä, J., Liang, X., Yu, X., Wang, Y., Kaartinen, H., Virtanen, J.-P., Hyyppä, J., 2020b. Accurate derivation of stem curve and volume using backpack mobile laser scanning. ISPRS J. Photogrammetry Remote Sens. 161, 246–262. https://doi.org/10.1016/j.isprsjprs.2020.01.018.

Hyyppä, J., Yu, X., Hakala, T., Kaartinen, H., Kukko, A., Hyyti, H., Muhojoki, J., Hyyppä, E., 2021. Under-canopy UAV laser scanning providing canopy height and stem volume accurately. Forests 12, 856. https://doi.org/10.3390/f12070856.

Jurjević, L., Liang, X., Gašparović, M., Balenović, I., 2020. Is field-measured tree height as reliable as believed – Part II, A comparison study of tree height estimates from conventional field measurement and low-cost close-range remote sensing in a deciduous forest. ISPRS J. Photogrammetry Remote Sens. 169, 227–241. https://doi.org/10.1016/j.isprsjprs.2020.09.014.

Kaartinen, H., Hyyppä, J., Vastaranta, M., Kukko, A., Jaakkola, A., Yu, X., Pyörälä, J., Liang, X., Liu, J., Wang, Y., Kaijaluoto, R., Melkas, T., Holopainen, M., Hyyppä, H., 2015. Accuracy of Kinematic positioning using global satellite navigation systems under forest canopies. Forests 6, 3218–3236. https://doi.org/10.3390/f6093218.

Kelbe, D., van Aardt, J., Romanczyk, P., van Leeuwen, M., Cawse-Nicholson, K., 2016. Marker-free registration of forest terrestrial laser scanner data pairs with embedded confidence metrics. IEEE Trans. Geosci. Rem. Sens. 54, 4314–4330. https://doi.org/10.1109/TGRS.2016.2539219.

Kukko, A., Kaijaluoto, R., Kaartinen, H., Lehtola, V.V., Jaakkola, A., Hyyppä, J., 2017. Graph SLAM correction for single scanner MLS forest data under boreal forest canopy. ISPRS J. Photogrammetry Remote Sens. 132, 199–209. https://doi.org/10.1016/j.isprsjprs.2017.09.006.

Liang, X., Hyyppä, J., 2013. Automatic stem mapping by merging several terrestrial laser scans at the feature and decision levels. Sensors 13, 1614–1634. https://doi.org/10.3390/s130201614.

Liang, X., Hyyppä, J., Kaartinen, H., Lehtomäki, M., Pyörälä, J., Pfeifer, N., Holopainen, M., Brolly, G., Francesco, P., Hackenberg, J., Huang, H., Jo, H.-W., Katoh, M., Liu, L., Mokroš, M., Morel, J., Olofsson, K., Poveda-Lopez, J., Trochta, J., Wang, D., Wang, J., Xi, Z., Yang, B., Zheng, G., Kankare, V., Luoma, V., Yu, X., Chen, L., Vastaranta, M., Saarinen, N., Wang, Y., 2018a. International benchmarking of terrestrial laser scanning approaches for forest inventories. ISPRS J. Photogrammetry Remote Sens. 144, 137–179. https://doi.org/10.1016/j.isprsjprs.2018.06.021.

Liang, X., Kankare, V., Hyyppä, J., Wang, Y., Kukko, A., Haggrén, H., Yu, X., Kaartinen, H., Jaakkola, A., Guan, F., Holopainen, M., Vastaranta, M., 2016. Terrestrial laser scanning in forest inventories. ISPRS J. Photogrammetry Remote Sens. 115, 63–77. https://doi.org/10.1016/j.isprsjprs.2016.01.006.

Liang, X., Kukko, A., Balenovic, I., Saarinen, N., Junttila, S., Kankare, V., Holopainen, M., Mokros, M., Surovy, P., Kaartinen, H., Jurjevic, L., Honkavaara, E., Nasi, R., Liu, J., Hollaus, M., Tian, J., Yu, X., Pan, J., Cai, S., Virtanen, J.-P., Wang, Y., Hyyppa, J., 2022. Close-range remote sensing of forests: the state of the art, challenges, and opportunities for systems and data acquisitions. IEEE Geosci. Remote Sens. Mag. 10, 32–71. https://doi.org/10.1109/MGRS.2022.3168135.

Liang, X., Kukko, A., Hyyppä, J., Lehtomäki, M., Pyörälä, J., Yu, X., Kaartinen, H., Jaakkola, A., Wang, Y., 2018b. In-situ measurements from mobile platforms: an emerging approach to address the old challenges associated with forest inventories. ISPRS J. Photogrammetry Remote Sens. 143, 97–107. https://doi.org/10.1016/j.isprsjprs.2018.04.019.

Liang, X., Litkey, P., Hyyppa, J., Kaartinen, H., Vastaranta, M., Holopainen, M., 2012. Automatic stem mapping using single-scan terrestrial laser scanning. IEEE Trans. Geosci. Rem. Sens. 50, 661–670. https://doi.org/10.1109/TGRS.2011.2161613.

Liang, X., Wang, Y., Pyörälä, J., Lehtomäki, M., Yu, X., Kaartinen, H., Kukko, A., Honkavaara, E., Issaoui, A.E.I., Nevalainen, O., Vaaja, M., Virtanen, J.-P., Katoh, M., Deng, S., 2019. Forest in situ observations using unmanned aerial vehicle as an alternative of terrestrial measurements. For. Ecosyst. 6, 20. https://doi.org/10.1186/s40663-019-0173-3.

Liu, J., Liang, X., Hyyppä, J., Yu, X., Lehtomäki, M., Pyörälä, J., Zhu, L., Wang, Y., Chen, R., 2017. Automated matching of multiple terrestrial laser scans for stem mapping without the use of artificial references. Int. J. Appl. Earth Obs. Geoinf. 56, 13–23. https://doi.org/10.1016/j.jag.2016.11.003.

Liu, Q., Wang, J., Ma, W., Zhang, J., Deng, Y., Shao, D., Xu, D., Liu, Y., 2021. Target-free ULS-TLS point-cloud registration for alpine forest lands. Comput. Electron. Agric. 190, 106460. https://doi.org/10.1016/j.compag.2021.106460.

Magnusson, M., Lilienthal, A., Duckett, T., 2007. Scan registration for autonomous mining vehicles using 3D-NDT. J. Field Robot. 24, 803–827. https://doi.org/10.1002/rob.20204.

Mulverhill, C., Coops, N.C., Tompalski, P., Bater, C.W., 2020. Digital terrestrial photogrammetry to enhance field-based forest inventory across stand conditions. Can. J. Rem. Sens. 46, 622–639. https://doi.org/10.1080/07038992.2020.1831376.

Myronenko, A., Song, Xubo, 2010. Point Set registration: coherent point drift. IEEE Trans. Pattern Anal. Mach. Intell. 32, 2262–2275. https://doi.org/10.1109/TPAMI.2010.46.

Ni, W., Sun, G., Guo, Z., Huang, H., 2011. A method for the registration of multiview range images acquired in forest areas using a terrestrial laser scanner. Int. J. Rem. Sens. 32, 9769–9787. https://doi.org/10.1080/01431161.2011.578597.

Paris, C., Kelbe, D., van Aardt, J., Bruzzone, L., 2017. A novel automatic method for the fusion of ALS and TLS Lidar data for robust assessment of tree crown structure. IEEE Trans. Geosci. Rem. Sens. 55, 3679–3693. https://doi.org/10.1109/TGRS.2017.2675963.

Pfeifer, N., Briese, C., 2007. Geometrical aspects of airborne laser scanning and terrestrial laser scanning. Int. Arch. Photogram. Rem. Sens. Spatial Inf. Sci. 36, 311–319.

Pierzchała, M., Giguère, P., Astrup, R., 2018. Mapping forests using an unmanned ground vehicle with 3D LiDAR and graph-SLAM. Comput. Electron. Agric. 145, 217–225. https://doi.org/10.1016/j.compag.2017.12.034.

Polewski, P., Yao, W., Cao, L., Gao, S., 2019. Marker-free coregistration of UAV and backpack LiDAR point clouds in forested areas. ISPRS J. Photogrammetry Remote Sens. 147, 307–318. https://doi.org/10.1016/j.isprsjprs.2018.11.020.

Pomerleau, F., Colas, F., Siegwart, R., 2015. A review of point cloud registration algorithms for mobile robotics. FNT Robot 4, 1–104. https://doi.org/10.1561/2300000035.

Pooja, A., Govindu, V.M., 2010. A multi-view extension of the ICP algorithm. In: Proceedings of the Seventh Indian Conference on Computer Vision, Graphics and Image Processing - ICVGIP '10. ACM Press, Chennai, India, pp. 235–242. https://doi.org/10.1145/1924559.1924591.

Pyörälä, J., Liang, X., Saarinen, N., Kankare, V., Wang, Y., Holopainen, M., Hyyppä, J., Vastaranta, M., 2019. Assessing branching structure for biomass and wood quality estimation using terrestrial laser scanning point clouds. Can. J. Rem. Sens. 44, 462–475. https://doi.org/10.1080/07038992.2018.1557040.

Qian, C., Liu, H., Tang, J., Chen, Y., Kaartinen, H., Kukko, A., Zhu, L., Liang, X., Chen, L., Hyyppä, J., 2016. An integrated GNSS/INS/LiDAR-SLAM positioning method for highly accurate forest stem mapping. Rem. Sens. 9, 3. https://doi.org/10.3390/rs9010003.

Saarinen, N., Kankare, V., Vastaranta, M., Luoma, V., Pyörälä, J., Tanhuanpää, T., Liang, X., Kaartinen, H., Kukko, A., Jaakkola, A., Yu, X., Holopainen, M., Hyyppä, J., 2017. Feasibility of terrestrial laser scanning for collecting stem volume information from single trees. ISPRS J. Photogrammetry Remote Sens. 123, 140–158. https://doi.org/10.1016/j.isprsjprs.2016.11.012.

Shao, J., Zhang, W., Mellado, N., Wang, N., Jin, S., Cai, S., Luo, L., Lejemble, T., Yan, G., 2020. SLAM-aided forest plot mapping combining terrestrial and mobile laser scanning. ISPRS J. Photogrammetry Remote Sens. 163, 214–230. https://doi.org/10.1016/j.isprsjprs.2020.03.008.

Tam, G.K.L., Cheng, Z.Q., Lai, Y.K., Langbein, F.C., Liu, Yonghuai, Marshall, D., Martin, R.R., Sun, X.F., Rosin, P.L., 2013. Registration of 3D point clouds and meshes: a survey from rigid to nonrigid. IEEE Trans. Visual. Comput. Graph. 19, 1199–1217. https://doi.org/10.1109/TVCG.2012.310.

Tremblay, J.-F., Béland, M., 2018. Towards operational marker-free registration of terrestrial lidar data in forests. ISPRS J. Photogrammetry Remote Sens. 146, 430–435. https://doi.org/10.1016/j.isprsjprs.2018.10.011.

Vaaja, M.T., Virtanen, J.-P., Kurkela, M., Lehtola, V., Hyyppä, J., Hyyppä, H., 2016. The effect of wind on tree stem parameter estimation using terrestrial laser scanning. ISPRS Ann. Photogramm. Remote Sens. Spat. Inform. Sci. III– 8, 117–122. https://doi.org/10.5194/isprsannals-III-8-117-2016.

Wang, Y., Kukko, A., Hyyppä, E., Hakala, T., Pyörälä, J., Lehtomäki, M., El Issaoui, A., Yu, X., Kaartinen, H., Liang, X., Hyyppä, J., 2021. Seamless integration of above- and under-canopy unmanned aerial vehicle laser scanning for forest investigation. For. Ecosyst. 8, 10. https://doi.org/10.1186/s40663-021-00290-3.

Wang, Y., Lehtomäki, M., Liang, X., Pyörälä, J., Kukko, A., Jaakkola, A., Liu, J., Feng, Z., Chen, R., Hyyppä, J., 2019a. Is field-measured tree height as reliable as believed – a comparison study of tree height estimates from field measurement, airborne laser scanning and terrestrial laser scanning in a boreal forest. ISPRS J. Photogrammetry Remote Sens. 147, 132–145. https://doi.org/10.1016/j.isprsjprs.2018.11.008.

Wang, Y., Pyörälä, J., Liang, X., Lehtomäki, M., Kukko, A., Yu, X., Kaartinen, H., Hyyppä, J., 2019b. In situ biomass estimation at tree and plot levels: what did data record and what did algorithms derive from terrestrial and aerial point clouds in boreal forest. Remote Sens. Environ. 232, 111309. https://doi.org/10.1016/j.rse.2019.111309.

Zhang, W., Chen, Y., Wang, H., Chen, M., Wang, X., Yan, G., 2016. Efficient registration of terrestrial LiDAR scans using a coarse-to-fine strategy for forestry applications. Agric. For. Meteorol. 225, 8–23. https://doi.org/10.1016/j.agrformet.2016.05.005.

Zhang, W., Shao, J., Jin, S., Luo, L., Ge, J., Peng, X., Zhou, G., 2021. Automated marker-free registration of multisource forest point clouds using a coarse-to-global adjustment strategy. Forests 12, 269. https://doi.org/10.3390/f12030269.